

Optimization and Mechanistic Characterization of Pyridopyrimidine Inhibitors of Bacterial Biotin Carboxylase

Logan Dane Andrews, Timothy R. Kane, Paola Dozzo, Cat M. Haglund, Darin J. Hilderbrandt, Martin S. Linsell, Timothy Machajewski, Glen McEnroe, Alisa W. Serio, Kenneth B. Wlasichuk, David B Neau, Svetlana Pakhomova, Grover L Waldrop, Marc Sharp, Joe Pogliano, Ryan Cirz, and Frederick Cohen

J. Med. Chem., **Just Accepted Manuscript** • DOI: 10.1021/acs.jmedchem.9b00625 • Publication Date (Web): 15 Jul 2019

Downloaded from pubs.acs.org on July 16, 2019

Just Accepted

“Just Accepted” manuscripts have been peer-reviewed and accepted for publication. They are posted online prior to technical editing, formatting for publication and author proofing. The American Chemical Society provides “Just Accepted” as a service to the research community to expedite the dissemination of scientific material as soon as possible after acceptance. “Just Accepted” manuscripts appear in full in PDF format accompanied by an HTML abstract. “Just Accepted” manuscripts have been fully peer reviewed, but should not be considered the official version of record. They are citable by the Digital Object Identifier (DOI®). “Just Accepted” is an optional service offered to authors. Therefore, the “Just Accepted” Web site may not include all articles that will be published in the journal. After a manuscript is technically edited and formatted, it will be removed from the “Just Accepted” Web site and published as an ASAP article. Note that technical editing may introduce minor changes to the manuscript text and/or graphics which could affect content, and all legal disclaimers and ethical guidelines that apply to the journal pertain. ACS cannot be held responsible for errors or consequences arising from the use of information contained in these “Just Accepted” manuscripts.

1
2
3 **TITLE:** Optimization and Mechanistic Characterization of Pyridopyrimidine Inhibitors of
4
5 Bacterial Biotin Carboxylase
6
7
8
9

10 **AUTHORS:** Logan D. Andrews^{*a}, Timothy R. Kane^a, Paola Dozzo^a, Cat M. Haglund^a, Darin J.
11
12 Hilderbrandt^a, Martin S. Linsell^a, Timothy Machajewski^a, Glen McEnroe^a, Alisa W. Serio^a,
13
14 Kenneth B. Wlasichuk^a, David B. Neau^b, Svetlana Pakhomova^b, Grover L. Waldrop^b, Marc
15
16 Sharp^c, Joe Pogliano^{c,d}, Ryan T. Cirz^{*a}, Frederick Cohen^a
17
18
19
20

21 ^aFormer employee of Achaogen Inc., 1 Tower Place, Suite 400, South San Francisco, CA 94080,
22
23 United States
24
25

26 ^bDepartment of Biological Sciences, Louisiana State University, Baton Rouge, LA 70803,
27
28 United States
29
30

31 ^cLinnaeus Bioscience Inc. 3210 Merryfield Row, San Diego, CA 92121, United States
32

33 ^dUniversity of California, San Diego 9500 Gilman Drive, La Jolla, 92093, United States
34
35
36
37

38 **ABSTRACT**

39
40 A major challenge for new antibiotic discovery is predicting the physicochemical properties that
41
42 enable small molecules to permeate Gram-negative bacterial membranes. We have applied
43
44 physicochemical lessons from previous work to redesign and improve the antibacterial potency of
45
46 pyridopyrimidine inhibitors of biotin carboxylase (BC) by up to 64-fold and 16-fold against *E. coli*
47
48 and *P. aeruginosa*, respectively. Antibacterial and enzyme potency assessments in the presence of
49
50 an outer membrane permeabilizing agent or in efflux-compromised strains indicate that penetration
51
52 and efflux properties of many redesigned BC inhibitors could be improved to various extents.
53
54
55
56
57
58
59
60

1
2
3 Spontaneous resistance to the improved pyridopyrimidine inhibitors in *P. aeruginosa* occurs at
4 very low frequencies between 10^{-8} to 10^{-9} . However, resistant isolates had alarmingly high MIC
5 shifts (16 to >128-fold) compared to the parent strain. Whole genome sequencing of resistant
6 isolates revealed that either BC target mutations or efflux pump overexpression can lead to the
7 development of high-level resistance.
8
9
10
11
12
13
14
15
16
17
18
19
20
21
22
23
24
25
26
27
28
29
30
31
32
33
34
35
36
37
38
39
40
41
42
43
44
45
46
47
48
49
50
51
52
53
54
55
56
57
58
59
60

INTRODUCTION

The spread of multi-drug resistant (MDR) bacteria presents a threat to our healthcare system. An analysis from the Centers for Disease Control indicates that approximately 23,000 people die annually in the US from these pathogens,¹ and more recent reports suggest this estimate is conservative.^{2,3} In the future, routine life-saving procedures such as the use of coronary stents, anti-cancer chemotherapy, and organ transplants could carry the risk of life-threatening bacterial infections. The situation is particularly alarming for MDR infections caused by the so-called Gram-negative “ESKAPE” pathogens - *E. coli*, *K. pneumoniae*, *A. baumannii*, and *P. aeruginosa*. This point is illustrated by the recent discovery of a strain of *K. pneumoniae* from a US ICU patient that is resistant to 26 antibiotics.⁴ To address this threat from MDR pathogens, a variety of new antibiotic discovery approaches are warranted including optimization of previously discovered compounds with existing, although sometimes low levels, of antibacterial potency.

One such previously discovered compound that serves as an enticing starting point for further optimization is the well-characterized biotin carboxylase (BC) inhibitor **1** that was identified in a high-throughput screen against a membrane-compromised, efflux pump-deficient strain of *E. coli* (*tolC*, *imp*).⁵ BC is a member of the fatty acid biosynthesis pathway (**Figure S1**) and has attracted attention over the past decade as a promising target for the development of novel, broad-spectrum antibiotics for Gram-negative bacterial infections.⁶⁻¹¹ The first committed step in this pathway is catalyzed by an essential cytoplasmic acetyl-CoA carboxylase multienzyme complex¹² (see also Supporting Information **Text S1**), and inhibitors of the BC active site of this complex have shown antibacterial activity against several Gram-negative species.^{5, 13-17} The BC active site is highly conserved across a number of bacterial pathogens, including *P. aeruginosa*, *E. coli*, and *H. influenzae*.¹⁸ While **1** lacks the potency to become a therapeutic agent, it is a promising

1
2
3 starting point for medicinal chemistry efforts because of its selective on-target activity, low
4 molecular weight, and available co-crystal structures with BC that enable structure-based
5
6 molecular design.
7
8

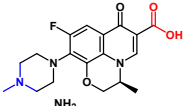
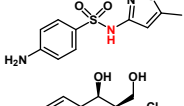
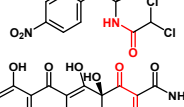
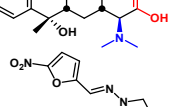
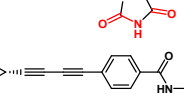
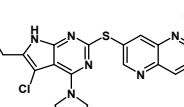
9
10 Inhibitors of BC must pass through both the outer and inner membranes of the Gram-
11 negative bacteria to reach this cytoplasmic-residing enzyme. The outer membrane bars the passage
12 of many exogenous small molecules. However, porins in the membrane allow some hydrophilic
13 molecules with a size and shape compatible with the diameter of the porin channels to diffuse into
14 the periplasm of the cell.¹⁹ Once in the periplasm, molecules must then pass through the
15 phospholipid inner membrane to reach cytoplasmic targets, a process favored by lower polarity.
16 Because the molecular properties of the outer and inner membranes differ, the two barriers act
17 orthogonally to greatly hinder the access of most potential inhibitors to their cytoplasmic target
18 sites. Even when a molecule successfully penetrates both membranes, efflux pumps that actively
19 remove foreign compounds from the cell further reduce the concentration of inhibitor reaching a
20 cytoplasmic target.^{20,21} These hurdles are major challenges to the development of small molecule
21 inhibitors designed to kill bacteria by acting within the cytoplasm.
22
23
24
25
26
27
28
29
30
31
32
33
34
35
36

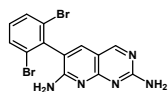
37 To address the challenge of discovering inhibitors that can readily access cytoplasmic
38 targets, retrospective chemoinformatic approaches have been used to evaluate the physicochemical
39 properties of molecules that accumulate effectively in Gram-negative cells.²²⁻²⁴ A pioneering
40 analysis by O'Shea and Moser, showed that, in general, antibiotics with Gram-negative activity
41 are significantly more polar (as measured by relative polar surface area and cLogD values) and
42 have more H-bond acceptor and donor atoms compared to a reference set of drugs from other
43 therapeutic areas.²⁵ For the subset of antibiotics that act against targets in the cytoplasm, the
44 physicochemical differences compared to the reference set were quite diverse, and less pronounced
45
46
47
48
49
50
51
52
53
54
55
56
57
58
59
60

for some classes of antibiotics, but still trended toward having higher overall polarity.^{24,25} However, a more recent assessment of Gram-negative cell compound accumulation that examined charge and polarity (cLogD) properties separately suggests that polarity alone is not predictive of cell accumulation.²⁶

To illustrate the physicochemical properties of cytoplasm-acting inhibitors that are sufficient for antibacterial potency, we compared a set of exemplar Gram-negative antibiotics (**Table 1**). These antibiotics have cLogD values ranging from -3.6 to 2.0 and all contain groups that ionize near physiological pH (7.4).

Table 1. Examples of cytoplasm-targeted Gram-negative agents with physicochemical properties of interest

| Compound | Structure ^c | MW (g/mol) | cLogD ^d | Charge class ^e |
|-----------------------|---|------------|--------------------|---------------------------|
| Levofloxacin |  | 361 | -2.0 | Zwitterionic |
| Trimethoprim |  | 290 | 1.1 | Basic |
| Sulfamethoxazole |  | 253 | -1.1 | Acidic |
| Chloramphenicol |  | 323 | 1.0 | Acidic |
| Tetracycline |  | 444 | -3.6 | Zwitterionic |
| Nitrofurantoin |  | 238 | -0.27 | Acidic |
| ACHN-975 ^a |  | 369 | 2.0 | Zwitterionic |
| Trius ^b |  | 420 | 1.3 | Basic |

1
2
3
4
5
6
7
8
9
10
11
12
13
14
15
16
17
18
19
20
21
22
23
24
25
26
27
28
29
30
31
32
33
34
35
36
37
38
39
40
41
42
43
44
45
46
47
48
49
50
51
52
53
54
55
56
57
58
59
60

395

3.3

Neutral

^aRef. 27. ^bRef. 28. ^cAcidic groups colored red; basic groups colored blue.

^dcLogD at pH 7.4. Calculated using ACD/Percepta GALAS algorithm,

Advanced Chemistry Development, Inc. ^eAt physiological pH = 7.4.

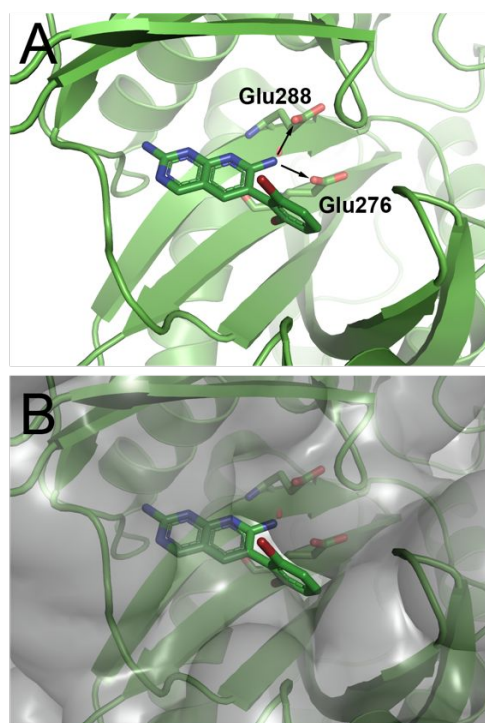
Comparing the property values in **Table 1** reveals that BC inhibitor **1** with a cLogD value of 3.3 is significantly less polar than the proven antibacterials. In addition and perhaps most importantly, **1** is the only compound in **Table 1** that does not contain an ionizable group. These comparisons suggest that the potency of **1** could be improved by increasing its polarity and installing ionizable groups with pK_a values in the physiological pH range. Further support for this approach was reported recently by the Hergenrother group, which showed that the addition of a primary amine to a molecule with a pK_a in the physiological pH range can significantly enhance cellular accumulation.^{26,29}

Herein, we report a structure-guided approach that was used to modulate the physicochemical properties of **1** to favor membrane penetration and efflux avoidance while simultaneously maintaining or improving BC target affinity, resulting in a significant overall improvement in antibacterial potency.

CHEMISTRY

Design Strategy. The previously determined structure of **1** bound to *E. coli* BC suggested two vectors allowing for physicochemical optimization while also permitting the retention, or even improvement of, BC target inhibition. The first vector points from the amine at the 7-position of the pyridopyrimidine ring toward two conserved glutamic acid residues that coordinate Mg^{2+} when

1
2
3 substrate ATP is bound (**Figure 1A**). The nearest oxygen atoms of these glutamic acid residue side
4 chains are 4.9 and 6.1 Å away from the 7-position nitrogen atom of **1**. We hypothesized that this
5 vector would provide an opportunity to place an ionizable amine group that would reduce the
6 cLogD value of the compound while also engaging the nearby glutamic acid residues via H-
7 bonding and/or electrostatic interactions. The second vector points off the dihalo-aromatic ring
8 through a small slot in the active site surface toward solvent (**Figure 1B**). We begin by focusing
9 our attention on the first vector at the 7-position of the aromatic ring system and subsequently
10 return to the second vector for further optimization. In the final phase of the campaign compounds
11 consisting of derivatizations at both vectors are presented.

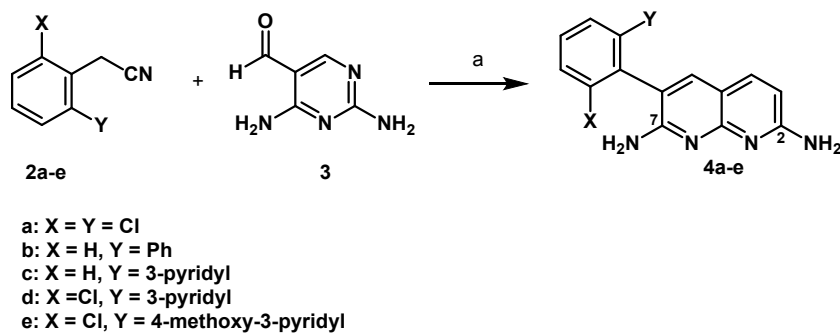


26
27
28
29
30
31
32
33
34
35
36
37
38
39
40
41
42
43
44
45
46
47
48
49
50 **Figure 1.** Compound **1** (carbon, green; nitrogen, blue; bromine, dark red; all rendered as sticks)
51 co-crystallized with *E. coli* BC at 2.1 Å as reported in Ref. **5** (PDB code 2V58). (A) View of
52 compound **1** in the BC active site showing the 7-position vector that points toward two proximal
53
54
55
56
57
58
59
60

1
2
3 glutamate residues as illustrated by the two arrows. The distance from the 7-position nitrogen atom
4 and nearest oxygen atoms of Glu288 and Glu276 are 4.9 and 6.1 Å, respectively. (B) View of the
5 solvent accessible surface representation, in transparent grey, of *E. coli* BC co-crystallized with **1**.
6
7 The second vector points off the dihalo-aromatic ring of **1** through a small slot in the active site
8 surface toward solvent. Images prepared using PyMOL.
9
10
11
12
13
14
15
16

17 **Synthesis.** Simple 2,7-diaminopyridopyrimidines such as **1** and **4a-e** are readily synthesized in
18 one step from aryl acetonitriles as shown in **Scheme 1**.
19
20
21
22
23

24 **Scheme 1.** Synthesis of 6-aryl pyridopyrimidines

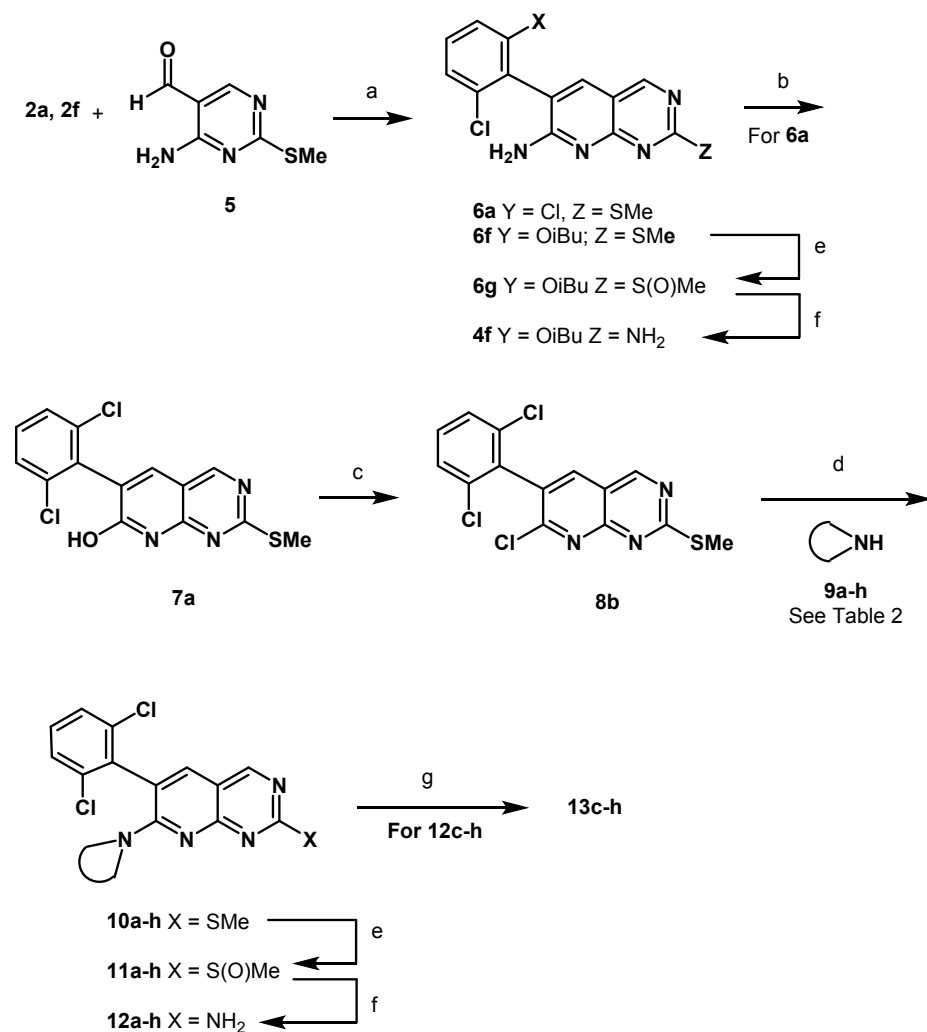


37 Reagents and conditions: (a) Base, solvent see Experimental Section.
38
39
40
41

42 To install an amine at the 7-position, we developed a novel synthetic route that allowed for
43 differentiation of the 2- and 7- positions as illustrated in **Scheme 2**. The route begins with a
44 condensation between aryl acetonitrile **2a** and pyrimidine **5**, wherein the eventual amine at the 2-
45 position is masked as a thiomethyl group. Following condensation, the 7-position is converted to
46 pyridone **7** by nitration and hydrolysis. Chlorination with POCl₃ provided **8** with a handle for
47 installation of various amines by simple S_NAr displacement. The sulfide was converted to an amine
48
49
50
51
52
53
54
55
56
57
58
59
60

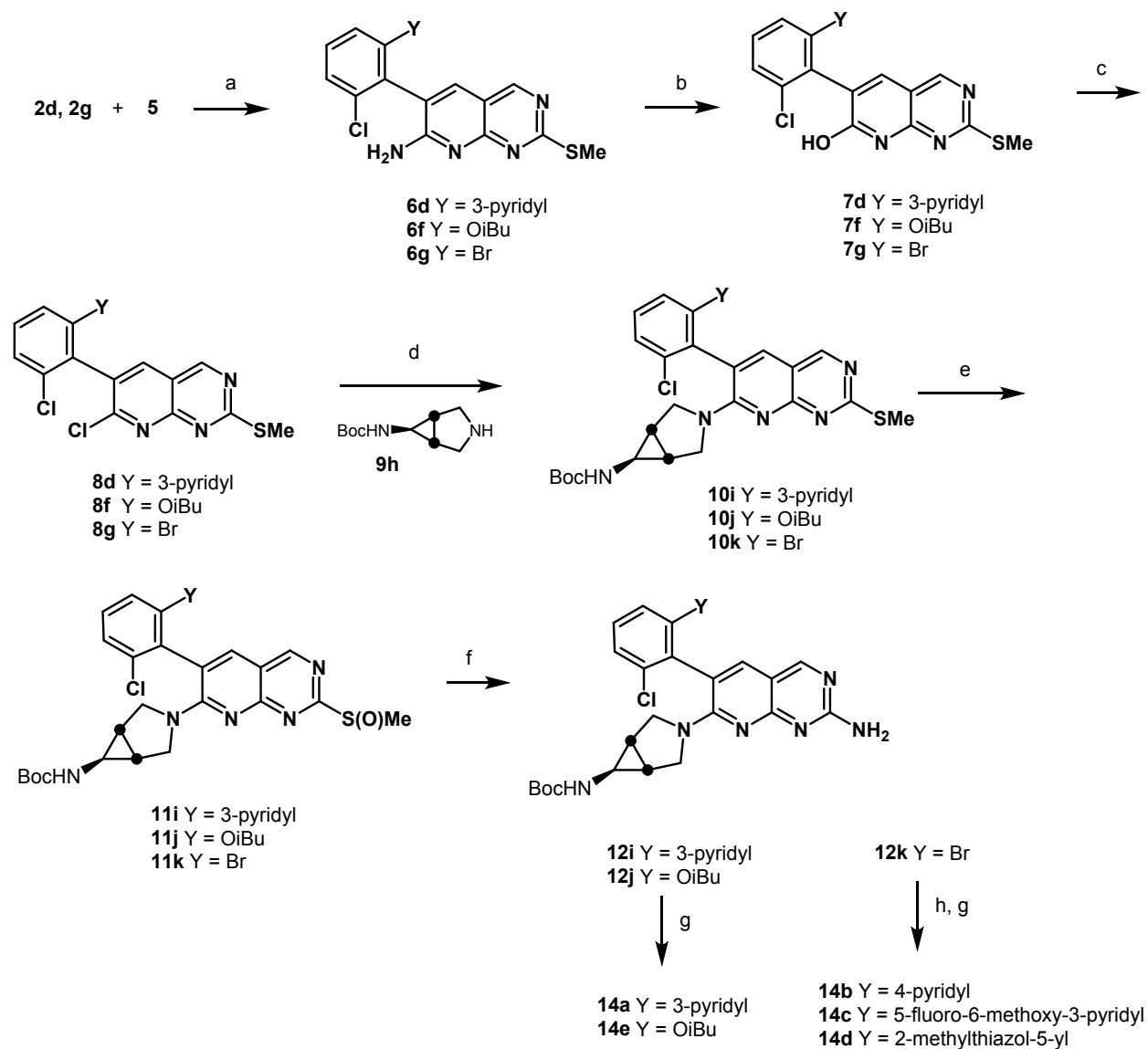
by oxidation to the sulfoxide and displacement with ammonia to provide analogs **12a-b**. If required, final Boc deprotection was affected with TFA, to afford inhibitors **13c-h**. This route could also be modified to allow for late-stage diversification via Suzuki reaction, as illustrated in **Scheme 3**, for the synthesis of compounds **14a-e**.

Scheme 2. Synthesis of Compounds **12a, b**, and **13c-h**



^aReagents and conditions: (a) NaH, DMF 45%; (b) NaNO₂, trifluoroacetic acid, 90%; (c) POCl₃, DMF (cat), 95 °C, 98%; (d) **9a-h**, MeCN, 1,4-dioxane, 80 °C; (e) mCPBA or Davies oxaziridine, DCM; (f) NH₃, MeOH, THF, 65 °C; (g) Trifluoroacetic acid, DCM.

Scheme 3. Synthesis of Compounds 14a–d



Reagents and conditions: (a) NaH, DMF; (b) NaNO₂, trifluoroacetic acid; (c) POCl₃, DMF (cat), 95 °C; (d) **9h**, MeCN, 1,4-dioxane, 80 °C; (e) mCPBA or Davies oxaziridine, DCM; (f) NH₃, MeOH, THF, 65 °C; (g) Trifluoroacetic acid, DCM; (h) R(BOH)₂, Pd(dppf)Cl₂, Na₂CO₃, dioxane, water, 80 °C.

RESULTS AND DISCUSSION

Structure-activity relationships for derivatives off the pyridopyrimidine 7-position.

Compound **4a** was chosen as the parent molecule for this first campaign because it is identical to **1** except for the substitution of the dibromo ring with a dichloro ring, which results in a slightly lower cLogD. In addition, the IC₅₀ value measured for **4a** is within 2-fold of the IC₅₀ value measured here for **1**, indicating that the ring substitution does not have a large impact on BC target-inhibition. As expected based on the potency reported for **1**, compound **4a** has limited microbiological activity against wild type (WT) ESKAPE pathogens *A. baumannii*, *E. coli*, and *K. pneumoniae*, and no activity against *P. aeruginosa* was detected (MIC >256µg/mL) (**Table 2**).

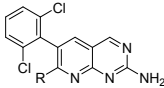
To test the ability of **4a** to penetrate the Gram-negative outer membrane, we conducted MIC assays in the presence and absence of the permeabilizing agent polymyxin B nonpeptide (PMBN). At the concentration used (8 µg/mL), PMBN does not have an antibacterial effect but is expected to render the outer membrane more permeable by interacting with and disrupting the negatively charged lipopolysaccharide (LPS) molecules that otherwise maintain the outer membrane order.³⁰ When PMBN is included, the MIC value of compound **4a** against *E. coli* is reduced 32-fold from 32 to 1 µg/mL. This significant enhancement of potency in the presence of PMBN suggests that when the outer membrane is compromised, a greater proportion of **4a** is able to reach the BC active site in the cytoplasm. By contrast, **ACHN-975** (**Table 1**), which also targets a cytoplasmic enzyme but has physicochemical properties that may be more conducive to membrane penetration, is only 2- to 4-fold more potent in the presence of PMBN suggesting that a greater proportion of **ACHN-975** readily crosses the outer membrane.

To test the contribution of efflux to the limited potency of **4a**, an *E. coli* ($\Delta tolC$) mutant was tested in the MIC assay. With this key efflux component deleted, the potency of **4a** is

1
2
3 strengthened by 64-fold (32 to 0.5 $\mu\text{g}/\text{mL}$), suggesting that WT *E. coli* uses a TolC-containing
4
5 efflux pump to dramatically reduce the intracellular concentration of **4a**. Similar results were
6
7 observed when comparing the MIC values of **4a** against WT and efflux-compromised strains of *P.*
8
9 *aeruginosa* (**Table 2**).

10
11
12 When PMBN was included with compound **4a** the MIC for *E. coli* ΔtolC strain is 0.25
13
14 $\mu\text{g}/\text{mL}$, the lowest value observed for all of the strains and conditions tested. Because the efflux-
15
16 compromised and WT strains are expected to have the same levels of LPS in their outer
17
18 membranes, we initially reasoned that PMBN should reduce the MIC by the same proportion for
19
20 both strains. Instead, the presence of PMBN induced only a 2-fold reduction in MIC against the
21
22 efflux-compromised strain (0.5 to 0.25 $\mu\text{g}/\text{mL}$), compared to a 32-fold reduction against the WT
23
24 strain (32 to 1 $\mu\text{g}/\text{mL}$). This disconnect suggests that when the outer membrane and efflux
25
26 mechanisms are both compromised, other properties of the bacterial cell and inhibitor, such as the
27
28 BC enzyme affinity and/or the ability of the inner membrane to exclude the inhibitor, become
29
30 limiting to the observed MIC potency.
31
32
33
34
35

36
37 Structural elaboration of **4a** at the 7-position of the pyridopyrimidine ring yielded
38
39 compounds **12a-b** and **13c-h** shown in **Table 2**. To test our structural expectation that groups at
40
41 this position could be readily accommodated by the BC enzyme, we measured the IC_{50} values
42
43 against purified *P. aeruginosa* BC. The results in **Table 2** show that the IC_{50} values measured are
44
45 all similar or better compared to **4a**, demonstrating that the 7-position modification does not disrupt
46
47 BC inhibition and in one case (**13h**) improves inhibition by nearly 10-fold.
48
49
50
51
52
53
54
55
56
57
58
59
60

Table 2. MIC values, IC₅₀ values, and physicochemical properties of interest for compounds elaborated at the 7-position


| | -R |  |  |  |  |  |  |  |  |  |
|--|----|---|---|--|---|---|---|---|---|---|
| | | 4a | 12a | 12b | 13c | 13d | 13e | 13f | 13g | 13h |
| Organism ^a | | | | | | | | | | |
| <i>A. baumannii</i> | | 256 | >256 | >64 | >256 | >256 | >256 | >256 | >128 | 128 |
| <i>E. coli</i> | | 32 | 64 | 32 | 16 | 32 | 64 | 16 | 32 | 2 |
| <i>K. pneumoniae</i> | | 64 | 256 | >64 | 256 | 256 | >256 | 64 | 128 | 8 |
| <i>P. aeruginosa</i> | | >256 | >256 | >64 | >256 | >256 | >256 | >256 | >128 | >256 |
| <i>E. coli</i> +PMBN | | 1 | 4 | 2 | 8 | 4 | 8 | 2 | 4 | 0.25 |
| <i>E. coli</i> ($\Delta tolC$) ^b | | 0.5 | 0.5 | 0.25 | 1 | 2 | 1 | 0.5 | 1 | 0.12 |
| <i>E. coli</i> ($\Delta tolC$) +PMBN | | 0.25 | 0.12 | 0.12 | 0.25 | 1 | 0.25 | 0.12 | 0.5 | 0.06 |
| <i>P. aeruginosa</i> ($\Delta mexAB, etc.$) ^c | | 16 | 256 | >64 | 256 | 256 | >64 | 64 | 64 | 8 |
| fold-change | | | | | | | | | | |
| <i>E. coli</i> +/-PMBN | | 32 | 16 | 16 | 2 | 8 | 8 | 8 | 8 | 8 |
| <i>E. coli</i> +/-efflux | | 64 | 128 | 128 | 16 | 16 | 64 | 32 | 32 | 16 |
| <i>E. coli</i> ($\Delta tolC$) +/-PMBN | | 2 | 4 | 2 | 4 | 2 | 4 | 4 | 2 | 2 |
| <i>P. aeruginosa</i> +/-efflux | | >16 | >1 | - | >1 | >1 | - | >4 | >2 | >32 |
| IC ₅₀ <i>P. aeruginosa</i> BC (nM) | | 320 | 170 | 140 | 190 | 440 | 83 | 64 | 320 | 33 |
| MW (g/mol) | | 307 | 403 | 390 | 405 | 407 | 405 | 389 | 403 | 387 |
| pK _a ^d | | 4.8 | (3.2) | 5.0 | 7.6 | 7.9 | 8.7 | 9.6 | 10.1 | 8.0 |
| clogD (pH 7.4) | | 2.8 | 2.9 | 3.5 | 2.3 | 1.6 | 0.6 | -0.1 | 0.8 | 2.7 |

^aThe strains of each bacterial species were as follows: *A. baumannii* (wild type) ATCC 19606; *E. coli* (wild type) DM4100; *K. pneumoniae* (wild type) ATCC 43816; *P. aeruginosa* (wild type) PAO1. ^bThe *E. coli* $\Delta tolC$ strain contains a targeted knockout of the efflux pump component TolC. ^cThe *P. aeruginosa* $\Delta mexAB, etc.$ strain contains targeted knockouts of efflux pumps MexAB-OprM,

1
2
3 MexCD-OprJ, and MexEF-OprN, and the efflux pump components MexXY are expected to be compromised by the absence of OprM.
4

5 ^dCalculated p*K*_a values are in parentheses.
6
7
8
9
10
11
12
13
14
15
16
17
18
19
20
21
22
23
24
25
26
27
28
29
30
31
32
33
34
35
36
37
38
39
40
41
42
43
44
45
46
47

1
2
3 In addition to having similar BC affinity compared to **4a**, the compounds **12a** and **12b**, also
4 have similar cLogD and pK_a values. Thus, it was expected that these compounds would perform
5 similarly to **4a** in the MIC panel. The MIC data for **12a** and **12b** in **Table 2** reflect these
6 expectations, with similarly low potency against WT strains and similarly strong MIC shifts
7 observed in the presence of PMBN and against the efflux mutants. These observations are
8 consistent with the premise that compounds with high cLogD values and no ionizable groups at
9 physiological pH values have difficulty entering cells and avoiding efflux.
10
11
12
13
14
15
16
17
18

19 To test the physicochemical hypothesis further, compound **12b** was modified with the
20 addition of a nitrogen atom with a pK_a value near physiological pH, resulting in amine-containing
21 compound **13c**. In addition to becoming ionizable, **13c** also has a modest decrease in cLogD.
22 Importantly, the BC affinity of **13c** remains relatively constant compared to the parent compound
23 so that any changes in potency can more likely be attributed to changes in the two important
24 physicochemical properties. **Table 2** shows that **13c** does not have a large increase in antibacterial
25 potency against WT strains. However, the presence of PMBN improves the potency of **13c** by only
26 2-fold, suggesting that it crosses the outer membrane more easily than compounds **4a** and **12a-b**,
27 which have MIC shifts of 16- to 32-fold in the presence of PMBN. Likewise, the 16-fold shift
28 observed with **13c** against the *E. coli* efflux-compromised strain compared to WT strain is much
29 lower than the 64- to 128-fold shifts seen with compounds **4a** and **12a-b**. The lower fold-change
30 suggests that compound **13c** also avoids efflux more readily than the neutral compounds with
31 higher cLogD values. Despite these apparent cellular penetration improvements and maintenance
32 of BC target affinity, the lack of corresponding improvement against WT strains suggests that **13c**
33 has lost potency due to some other difference(s) compared to **4a** and **12a-b**. While currently
34 untested, one hypothesis is that **13c** has a reduced ability to cross the Gram-negative inner
35
36
37
38
39
40
41
42
43
44
45
46
47
48
49
50
51
52
53
54
55
56
57
58
59
60

1
2
3 membrane relative to **4a** and **12a-b**. The direct measurement of the accumulation of compound
4
5 inside the cell could help test this hypothesis.
6

7
8 Further derivatives of **13c** were designed to increase the pK_a and lower the cLogD, again
9
10 with the expectation that such changes would improve outer membrane penetration and efflux
11 avoidance. Contrary to this expectation, these derivatives (**13d-g** in **Table 2**) all have higher MIC
12 shifts in the presence of PMBN compared to **13c** (8-fold versus 2-fold, respectively). In addition,
13
14 all had equal or larger MIC shifts against the efflux compromised strain compared to **13c**. These
15
16 observations suggest that an unknown counteracting property of these derivatives reduce their
17
18 ability to penetrate the outer membrane and avoid efflux relative to **13c**. One possible explanation
19
20 is that the basicity of the amines of **13d-g** is too high since they all have pK_a values greater than
21
22 **13c**. If true, this would suggest there is a narrow pK_a range for this scaffold to achieve optimal
23
24 cellular penetration. When the majority of the compound population is positively charged at
25
26 physiological pH, as is the case when the pK_a is >8 , the membrane penetration and efflux avoidance
27
28 properties of the compounds may get worse despite relatively low cLogD values. While this model
29
30 also remains untested, we focused our further medicinal chemistry efforts in this series on making
31
32 compounds with amine pK_a values less than 8.
33
34
35
36
37
38
39

40 After further rounds of elaboration at the 7-position, the most potent compound against the
41
42 WT strains identified **13h**, which contained an amino azabicyclohexane group with a pK_a value of
43
44 8. This compound had similar physicochemical properties as compounds **13d-g** and yielded similar
45
46 MIC shifts in the presence of PMBN and against the efflux compromised strain. However, **13h**
47
48 achieved the lowest MIC values against the WT strains of interest (except against *P. aeruginosa*,
49
50 which remained above the measurable range), presumably due to its approximately 10-fold
51
52 improvement in BC target affinity compared to the parent **4a**. The resiliency of the WT *P.*
53
54
55
56
57
58
59
60

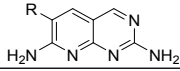
1
2
3 *aeruginosa* strain was not unexpected as this species is known to have a less permeable membrane
4 and a more extensive efflux system compared to the other ESKAPE pathogens tested here.³¹⁻³⁵
5
6
7
8
9

10 **Structure-activity relationships of slot position derivatives.** In an effort to further improve the
11 potency of parent compound **4a**, we turned our attention to the second vector of interest pointing
12 off the dihalo-aromatic ring (**Figure 1B**). Structural elaboration at this position occurred in two
13 phases. The first phase involved the addition of various aryl groups off of the dibromo aromatic
14 ring that were designed to fit within the small surface slot of the BC active site (**Figure 1B**). These
15 modifications did not contain groups capable of ionizing near physiological pH nor did they result
16 in large reductions to the cLogD so it was not expected that these compounds would have enhanced
17 membrane penetration or efflux avoidance.
18
19
20
21
22
23
24
25
26
27

28 These new compounds were tested against our MIC panel to assess cellular entry properties
29 and overall potency (**Table 3**). In accordance with expectations, this set of compounds had large
30 MIC shifts when PMBN was present, similar to parent compounds **1** and **4a**. These compounds
31 were also much more potent against the *E. coli* efflux-compromised strain relative to the WT strain,
32 with MIC shifts ranging from 64- to >512-fold. These observations support the prediction that this
33 set of compounds would retain relatively poor outer membrane permeability and high efflux
34 potential because of unoptimized physicochemical properties. However, we note that compound
35 **4c** has a cLogD value a full unit lower than parent **1**, yet the MIC fold-shift for this compound
36 suggests no improvement in either outer membrane penetration or efflux avoidance. While this
37 reduction in cLogD value may not be large enough to yield predictable penetration and efflux
38 avoidance improvements, it may also be that introduction of polarity at this particular position on
39 the molecule is ineffective for reasons not captured by the simple expectation based solely on bulk
40
41
42
43
44
45
46
47
48
49
50
51
52
53
54
55
56
57
58
59
60

1
2
3 physicochemical properties. Given that **4c** has the same cLogD as **13c**, which did not show large
4
5 MIC shifts in the presence of PMBN or when efflux was compromised, it may be that the presence
6
7 of an ionizable amine, as on **13c** and not **4c**, is the more important property in determining cellular
8
9 accumulation compared to the cLogD parameter.
10
11
12
13
14
15
16
17
18
19
20
21
22
23
24
25
26
27
28
29
30
31
32
33
34
35
36
37
38
39
40
41
42
43
44
45
46
47
48
49
50
51
52
53
54
55
56
57
58
59
60

Table 3. MIC values, IC₅₀ values, and physicochemical properties of interest for compounds elaborated at the slot-position



| | -R |  |  |  |  |  |  |
|---|--|---|---|--|---|---|---|
| | Organism ^a | 1 | 4b | 4c | 4d | 4e | 4f |
| MIC (mg L ⁻¹) | <i>A. baumannii</i> | 128 | >256 | >256 | >256 | >256 | >128 |
| | <i>E. coli</i> | 32 | >256 | 256 | 8 | 8 | 32 |
| | <i>K. pneumoniae</i> | 64 | >256 | 256 | 32 | >16 | >128 |
| | <i>P. aeruginosa</i> | >256 | >256 | >256 | >256 | >256 | >128 |
| | <i>E. coli</i> +PMBN | 0.5 | 2 | 4 | 0.5 | 0.25 | 1 |
| | <i>E. coli</i> ($\Delta tolC$) ^b | 0.5 | 0.5 | 2 | 0.12 | 0.06 | 0.25 |
| | <i>E. coli</i> ($\Delta tolC$) +PMBN | 0.12 | 0.25 | 0.5 | 0.06 | 0.03 | ≤0.06 |
| | <i>P. aeruginosa</i> ($\Delta mexAB, etc.$) ^c | 16 | >256 | 16 | 4 | 8 | 32 |
| fold-change | <i>E. coli</i> +/-PMBN | 64 | >128 | 64 | 16 | 32 | 32 |
| | <i>E. coli</i> +/-efflux | 64 | >512 | 128 | 64 | 128 | 128 |
| | <i>E. coli</i> ($\Delta tolC$) +/-PMBN | 4 | 2 | 4 | 2 | 2 | >4 |
| | <i>P. aeruginosa</i> +/-efflux | >16 | - | >16 | >64 | >32 | >4 |
| IC ₅₀ <i>P. aeruginosa</i> BC (nM) | 180 | 79 | 130 | 36 | 32 | 93 | |
| MW (g/mol) | 395 | 313 | 314 | 349 | 379 | 344 | |
| pK _a ^d | 4.8 | (4.7) | (4.9) | (4.4) | (3.8) | (3.9) | |
| clogD (pH 7.4) | 3.3 | 3.2 | 2.3 | 2.9 | 2.6 | 2.9 | |

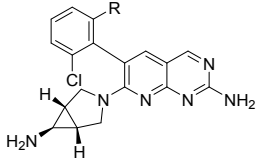
^aThe strains of each bacterial species were as follows: *A. baumannii* (wild type) ATCC 19606; *E. coli* (wild type) DM4100; *K. pneumoniae* (wild type) ATCC 43816; *P. aeruginosa* (wild type) PAO1. ^bThe *E. coli* $\Delta tolC$ strain contains a targeted knockout of the efflux pump component TolC. ^cThe *P. aeruginosa* $\Delta mexAB, etc.$ strain contains targeted knockouts of efflux pumps MexAB-OprM, MexCD-OprJ, and MexEF-OprN, and the efflux pump components MexXY are expected to be compromised by the absence of OprM. ^dCalculated pK_a values are in parentheses.

To assess the effect of the structural changes off the dibromo aromatic ring on target BC inhibition, IC₅₀ values were measured using purified *P. aeruginosa* BC. As these derivatives were designed to sterically fit into a small slot extending from the BC active site but not make new

1
2
3 specific interactions, it was expected that the IC₅₀ values of the elaborated compounds would be
4 quite similar to parent compound **1**. As expected, the IC₅₀ values reported in **Table 3** are
5 approximately equal to or lower by up to 6-fold of **1**, indicating that the introduction of additional
6 ring systems at this position do not cause major disruptions to target inhibition. Wary of the
7 potential for the additional aromatic ring to reduce solubility, it was discovered that certain
8 aliphatic groups, such as isobutyl **4f**, could also fit the slot position and afford activity against the
9 enzyme.
10
11
12
13
14
15
16
17
18

19 For the final phase of the structural elaboration off the dihalo-aromatic ring we chose a
20 starting scaffold with the best amine-containing group identified during the derivatization
21 campaign at the 7-position of the pyridopyrimidine ring, **13h**. The first two related compounds in
22 the series, **14a** and **14b** (**Table 4**), maintained the physicochemical properties of the parent
23 compound **13h** and showed an improvement in BC inhibition, with IC₅₀ values recorded at the
24 lower limit of detection of ≤15 nM – an improvement of ≥2-fold relative to the parent **13h**. This
25 BC target inhibition improvement could be responsible for the small MIC improvements observed
26 against the WT strains (with the exception of *A. baumannii*). No substantially different MIC shifts
27 were observed in the presence of PMBN or when efflux was compromised, as expected given that
28 **14a** and **14b** have pK_a and cLogD values similar to the parent comparator **13h** and all compounds
29 contain an ionizable amine.
30
31
32
33
34
35
36
37
38
39
40
41
42
43
44
45
46
47
48
49
50
51
52
53
54
55
56
57
58
59
60

Table 4. MIC values, IC₅₀ values, and physicochemical properties of interest for compounds elaborated in the final phase of the medicinal chemistry campaign

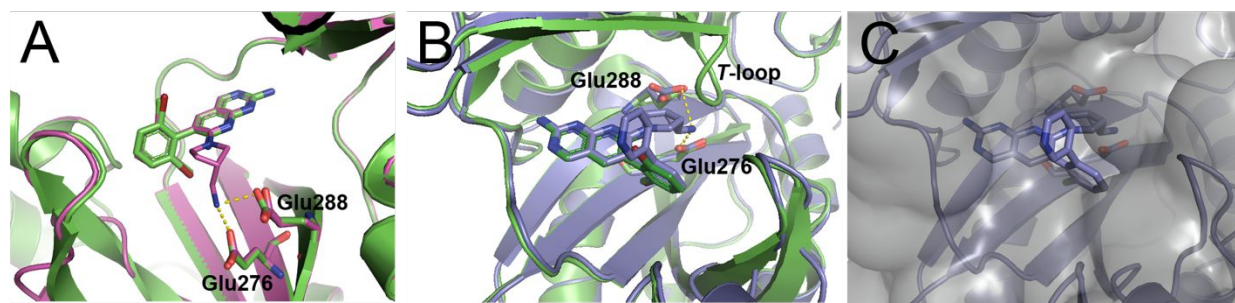


| | -R |  |  |  |  |  |
|--|----|---|---|--|---|---|
| | | 14a | 14b | 14c | 14d | 14e |
| Organism ^a | | | | | | |
| <i>A. baumannii</i> | | >256 | 128 | 32 | 128 | 32 |
| <i>E. coli</i> | | 1 | 1 | 1 | 0.5 | 2 |
| <i>K. pneumoniae</i> | | 8 | 4 | 4 | 2 | 8 |
| <i>P. aeruginosa</i> | | 256 | 128 | 128 | 128 | >64 |
| <i>E. coli</i> +PMBN | | 0.12 | 0.12 | 0.06 | 0.03 | 0.06 |
| <i>E. coli</i> ($\Delta tolC$) ^b | | 0.03 | 0.03 | 0.015 | 0.008 | 0.03 |
| <i>E. coli</i> ($\Delta tolC$) +PMBN | | 0.008 | 0.015 | 0.008 | 0.004 | 0.015 |
| <i>P. aeruginosa</i> ($\Delta mexAB, etc.$) ^c | | 1 | 2 | 2 | 1 | 8 |
| fold-change | | | | | | |
| <i>E. coli</i> +/-PMBN | | 8 | 8 | 16 | 16 | 32 |
| <i>E. coli</i> +/-efflux | | 32 | 32 | 64 | 64 | 64 |
| <i>P. aeruginosa</i> +/-efflux | | 256 | 64 | 64 | 128 | >8 |
| IC ₅₀ <i>P. aeruginosa</i> BC (nM) | | ≤15 | ≤15 | ≤15 | ≤15 | ≤15 |
| MW (g/mol) | | 430 | 430 | 478 | 450 | 425 |
| pK _a ^d | | 8.4 | (8.1) | (8.1) | (8.1) | 8.1 |
| cLogD (pH 7.4) | | 2.5 | 2.5 | 2.4 | 2.6 | 2.8 |

^aThe strains of each bacterial species were as follows: *A. baumannii* (wild type) ATCC 19606; *E. coli* (wild type) DM4100; *K. pneumoniae* (wild type) ATCC 43816; *P. aeruginosa* (wild type) PAO1; *S. aureus* (wild type) ATCC 29213. ^bThe *E. coli* $\Delta tolC$ strain contains a targeted knockout of the efflux pump component TolC. ^cThe *P. aeruginosa* $\Delta mexAB, etc.$ strain contains targeted knockouts of efflux pumps MexAB-OprM, MexCD-OprJ, and MexEF-OprN, and the efflux pump components MexXY are expected to be compromised by the absence of OprM. ^dCalculated pK_a values are in parentheses.

1
2
3 The next compounds in the series, **14c-14e**, all maintained BC IC₅₀ values below 15 nM
4 and achieved the most potent microbiological activity observed in the series. As these compounds
5 also maintained the general physicochemical properties of the starting scaffold, the MIC shifts
6 observed in the presence of PMBN or against the efflux compromised strain were similar to the
7 shifts observed with the parent compound.
8
9
10
11
12
13
14
15
16

17 **Structural Biology.** To assess the structural consequences of the 7-position modifications, the X-
18 ray co-crystal structure of **13f** with the WT BC enzyme from *E. coli* was solved at 2.06 Å (see
19 **Table S1** for crystallographic statistics). **Figure 2A** shows that the pyridopyrimidine ring scaffold
20 of **13f** occupies the same position as the previously reported structure of **1**.⁵ Thus, neither the
21 dibromo- to dichloro-substitution nor the modification off the 7-position altered the scaffold
22 binding position in the BC active site pocket.
23
24
25
26
27
28
29
30
31
32



33
34
35
36
37
38
39
40
41
42
43 **Figure 2.** BC co-crystal structures of new pyridopyrimidine inhibitors overlaid with previously
44 identified parent compound **1** co-crystallized with *E. coli* BC (shown in green; PDB 2V58). (A)
45 Compound **13f** (carbon, magenta; nitrogen, blue; chlorine, light green; all rendered as sticks) co-
46 crystallized with *E. coli* BC at 2.06 Å (magenta ribbon cartoon; PDB code 6OI9). The core
47 pyridopyrimidine scaffold of **13f** is found in the identical position as that of parent compound **1**.
48 The 7-position moiety extending off **13f** points toward the conserved glutamate residues placing
49
50
51
52
53
54
55
56
57
58
59
60

1
2
3 its proximal amine group nitrogen atom 3.16 and 2.17 Å in mol A and 2.97 and 2.65 Å in mol B
4
5 away from the nearest oxygen atoms of the carboxylate groups of Glu288 and Glu276,
6
7 respectively. (B) Compound **14a** (carbon, light blue; nitrogen, blue; chlorine, light green; all
8
9 rendered as sticks) co-crystallized with the *H. influenzae* BC at 2.5 Å (light blue-ribbon cartoon;
10
11 PDB code 6OI8). The *T*-loop (Ref. **36**) in the *H. influenzae* crystal structure is presumably
12
13 disordered, as observed previously in other BC crystal structures (Ref. **37**) and not represented by
14
15 the ribbon cartoon. The core pyridopyrimidine scaffold of **14a** is found in the identical position as
16
17 that of parent compound **1**. The 7-position moiety extending off **14a** points toward the conserved
18
19 glutamate residues placing its proximal amine group nitrogen atom 3.29 and 2.91 Å away from
20
21 the nearest oxygen atoms of the carboxylate groups of Glu288 and Glu276, respectively. (C) The
22
23 vector of **14a** that extends off the dihalo-aromatic ring is positioned, as expected, within the small
24
25 slot in the active site surface as shown by the partially transparent solvent accessible surface
26
27 representation in grey. Images prepared using PyMOL.
28
29
30
31
32
33
34

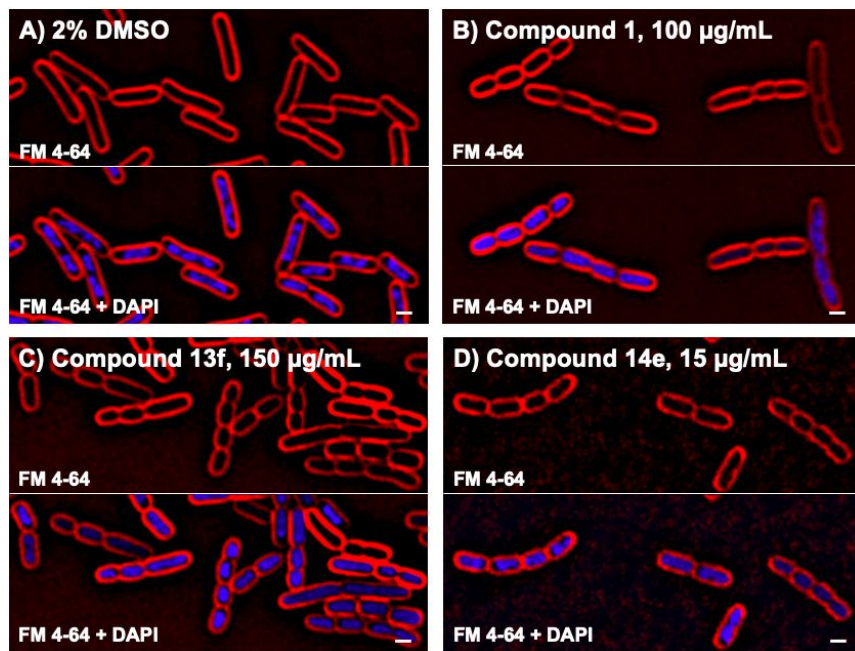
35
36 Consistent with our hypothesis based on the structure of **1**, the 7-position modification of
37
38 **13f** extends further into the interior of the BC enzyme placing the distal amine within H-bonding
39
40 distance to Glu288 and Glu276. Consistent with this possibility, the IC₅₀ results show a 5-fold
41
42 improvement in the inhibition of **13f** compared to **4a**, possibly reflecting the binding contribution
43
44 of the new H-bond interactions to the conserved glutamate residues that are formed by **13f**;
45
46 however, mutation studies involving both glutamate residues would be needed to more definitively
47
48 assign the binding affinity consequences of the 7-position modification.
49
50

51
52 To investigate the structural consequences of modifications off the dihalo ring, the crystal
53
54 structure of **14a** in complex with WT BC enzyme from *H. influenzae* was solved at 2.5 Å (**Figure**
55
56
57
58
59
60

1
2
3 **2B and C**; see **Table S1** for crystallographic statistics). The active site of the *H. influenzae* BC
4 enzyme is nearly identical to the other Gram-negative species of interest.^{5,18} The structure shows
5 that the pyridopyrimidine ring scaffold of **14a** occupies the same position as **13f** and the previously
6 reported structure of **1** demonstrating that the pyridyl modification off the dihalo ring does not
7 alter the binding conformation of the core ring system. This modification is positioned, as intended,
8 within the slot region of the BC active site, potentially making packing interactions to the residues
9 in the walls of the slot (**Figure 2C**). The structure also shows that the 7-position moiety of **14a**
10 extends toward the conserved Glu288 and Glu276 residues positioning the primary amine of **14a**
11 within H-bonding distance to the two acid residues (**Figure 2B**). Thus, both modifications found
12 on **14a** had the intended structural consequences.
13
14
15
16
17
18
19
20
21
22
23
24
25
26
27

28 **Bacterial Cytological Profiling.** The optimization of antibacterial compounds may be
29 compromised by off-target activity that would complicate interpretation of structure-activity
30 relationships.³⁸ To test that the improved antibacterial potency of the novel BC inhibitors was due
31 to on-target activity, Bacterial Cytological Profiling was used. Briefly, this technique uses high
32 resolution fluorescence microscopy to compare the effects on cytological structure of novel
33 antibiotics to a set of reference control antibiotics with known targets.^{39,40} Compounds that inhibit
34 different pathways generate reproducible and distinct cytological signatures that can be used to
35 infer the mechanism of action of unknown compounds.³⁹⁻⁴⁴ When *E. coli* cells were treated with
36 the previously reported BC inhibitor **14** at ~3-fold the MIC for 2 hours they formed short chains of
37 3 to 8 cells, a phenotype that is characteristic of lipid biogenesis inhibitors (**Figure 3**). Two novel
38 inhibitors, **13f** and **14e**, were tested in the profiling assay. It was found that both showed
39
40
41
42
43
44
45
46
47
48
49
50
51
52
53
54
55
56
57
58
59
60

1
2
3 cytological profiles very similar to each other and to parent compound **1** suggesting that they
4
5 inhibit the same target *in vivo*.
6
7
8
9



10
11
12
13
14
15
16
17
18
19
20
21
22
23
24
25
26
27
28
29
30
31 **Figure 3. Cells treated with BC inhibitors produce chains of**
32 **cells.** Cells were treated with either DMSO or compound at the
33 indicated concentrations for 2 hours. The top panel shows FM4-64
34 stained cell membranes (red) and the bottom panel shows both cell
35 membranes and DNA stained with DAPI (blue). Scale bar equals 1
36
37
38
39
40
41
42
43
44
45
46
47
48
49
50
51
52
53
54
55
56
57
58
59
60
micron.

57
58
59
60
Selectivity characterization. Compound **1** is a member of a class of compounds that were originally identified as inhibitors of VEGFR2 and FGFR1 eukaryotic protein kinases.⁴⁵ However, in the original report,⁵ **1** was shown to have acceptable selectivity for bacterial BC over these and 28 other eukaryotic protein kinases. To test if the potency improvements of the derivative

compounds synthesized in the current work came at the expense of losses in selectivity, two particularly promising compounds, **14a** and **14e**, were subjected to a similar panel of kinases. Compounds were profiled at a single concentration of 25 μ M in the Z'-LYTE kinase activity assay at Invitrogen. The results are shown in **Table 5**. Compared to parent compound **1**, the novel compounds retain excellent and even improved selectivity against this panel of kinases.

Table 5. Percent inhibition of eukaryotic kinases at a compound concentration of 25 μ M

| kinase | compound | | |
|---------------------------|----------|------------|------------|
| | 1 | 14a | 14e |
| ABL1 | 97 | 38 | 30 |
| FYN | 93 | 12 | 12 |
| SRC | 93 | 8 | 8 |
| BTK | 92 | 16 | 32 |
| FGFR1 | 78 | 57 | 60 |
| EGFR (ErbB1) | 58 | 65 | 6 |
| MAP4K4 (HGK) | 52 | 21 | 24 |
| NTRK1 (TRKA) | 47 | 47 | 40 |
| MAPK1 (ERK2) | 26 | 1 | 6 |
| MAPK14 (p38 alpha) Direct | 24 | 1 | 5 |
| MET (cMet) | 21 | 7 | 15 |
| AURKA (Aurora A) | 20 | 9 | 8 |
| PAK4 | 20 | 25 | 23 |
| CDK1/cyclin B | 18 | 4 | 4 |
| CSNK1D (CK1 delta) | 16 | 3 | 3 |
| CHEK2 (CHK2) | 13 | 20 | 67 |
| MAPKAPK2 | 10 | 26 | 21 |
| SGK (SGK1) | 7 | 32 | 32 |
| INSR | 6 | 3 | 3 |
| GSK3B (GSK3 beta) | 6 | 4 | 7 |
| IKBKB (IKK beta) | 5 | 5 | 8 |
| AKT1 (PKB alpha) | 4 | 6 | 7 |
| CSNK2A1 (CK2 alpha 1) | 4 | 0 | 1 |
| PDK1 Direct | 3 | 0 | 0 |
| PRKCZ (PKC zeta) | 0 | 5 | -8 |
| CHEK1 (CHK1) | -1 | 28 | 42 |
| IKBKE (IKK epsilon) | -7 | 3 | 0 |

Determination of resistance liabilities. One concern with inhibitors targeting a single enzyme is that single point mutations in the target enzyme may lead to high-level resistance. Due to the high

1
2
3 bacterial burden and error-prone replication, it is feasible for bacteria to sample every possible
4 point mutation during the course of an infection. If a single-point mutation can disrupt inhibitor
5 binding without drastically impairing enzyme function then the infection will become resistant [for
6 example see Ref. 46]. Efflux-mediated resistance is more common than target-based resistance,
7 but upregulation of a single efflux system usually has a moderate impact on potency.
8
9

10
11 To determine whether high-level resistance to our inhibitors could arise in *P. aeruginosa*,
12 we selected for spontaneous resistant mutants in the efflux-compromised *P. aeruginosa* strain. The
13 lack of genes encoding the three major antibiotic efflux systems increases the likelihood of
14 identifying rare mutations in other genes. However, it should be noted that *P. aeruginosa* encodes
15 additional efflux systems that can contribute to resistance.
16
17

18
19 We selected for mutants on agar plates containing 4-, 8-, or 16-fold the MIC of compounds
20 **1**, **14a**, or **14e**. The spontaneous mutation frequency of these compounds in this strain background
21 was similar, ranging from 2×10^{-9} for **14e** to 9×10^{-9} for **14a** at 8-fold above the MIC. These
22 frequencies are low and similar to the frequencies observed for compound **1** previously.⁵ We note
23 however that spontaneous mutation frequencies would likely be much higher for a WT *P.*
24 *aeruginosa* strain carrying the full suite of efflux systems as these additional components can also
25 mutate to more efficiently efflux lethal compounds.
26
27

28
29 Several resistant colonies of the efflux-compromised *P. aeruginosa* strain were found to
30 harbor mutations in the BC coding sequence. These mutations encoded changes to amino acids
31 Leu278 and Ile437, which are located in the BC active site according to a structure of the *P.*
32 *aeruginosa* enzyme in complex with a substrate analog (PDB: 2VQD).¹⁸ Both residues are highly
33 conserved across BC species including *E. coli* and *H. influenzae*.^{5,18} The I437N and I437T
34 mutations identified here have also been observed previously when efflux-compromised strains of
35
36
37
38
39
40
41
42
43
44
45
46
47
48
49
50
51
52
53
54
55
56
57
58
59
60

E. coli and *H. influenzae* were grown in the presence of **1**.⁵ The L278F mutation observed here in *P. aeruginosa* was not identified in either the *E. coli* or *H. influenzae* enzymes.⁵ However, several other active site mutations were observed in *E. coli* and *H. influenzae* that were not observed in the current study, possibly because not enough resistant colonies were screened to exhaustively identify all possible mutants. If this were the case, additional screening would eventually reveal the same set of resistance conferring mutants for all BC species. Alternatively, the different sets of active site mutations observed in the BC enzymes from different species may reflect the influence of subtle BC structural differences that result in truly different sets of possible resistance-conferring mutations.

All three *P. aeruginosa* BC active site mutations isolated in this study have markedly stronger effects on the potency of **14a** compared to **14e** (Table 6). The L278F mutation raised the MIC of **14a** by 256-fold above the MIC of the parent strain, while both I437 mutations raised the MIC 128-fold. In contrast, **14e** was less affected by all three mutations, showing 8-fold MIC shifts above the parent strain.

Table 6. MIC changes conferred by spontaneous *P. aeruginosa* mutations

| Strain | MIC (mg L ⁻¹) | | | fold-change from WT | | |
|----------------------------|---------------------------|------------|------------|---------------------|------------|------------|
| | 1 | 14a | 14e | 1 | 14a | 14e |
| WT background ^a | 16 | 1 | 8 | (1) | (1) | (1) |
| BC L278F | 128 | 256 | 64 | 8 | 256 | 8 |
| BC I437N | >128 | 128 | 64 | >8 | 128 | 8 |
| BC I437T | >128 | 128 | 64 | >8 | 128 | 8 |
| MexT F201I | >128 | 2 | 8 | >8 | 2 | 1 |
| MexT P202L | >128 | 2 | 8 | >8 | 2 | 1 |
| MexT V226L | >128 | 1 | 8 | >8 | 1 | 1 |
| INV(<i>mexA-mexZ</i>) | >128 | 32 | 32 | >8 | 32 | 4 |

^a*P. aeruginosa* Δ *mexAB-oprM*, Δ *mexCD-oprJ*, Δ *mexEF-oprN*

[PAM1626 from Ref. 47]

1
2
3
4
5
6 Examination of the **14a** *H. influenzae* BC X-ray co-crystal structure overlaid with the
7
8 previously reported *P. aeruginosa* BC with substrate analog co-crystal structure¹⁸ offers a
9
10 speculative model for how the resistance-conferring mutations might disrupt inhibitor binding but
11
12 not significantly impact substrate turnover (**Figure 4**). In the *H. influenzae* structure, the
13
14 pyridopyrimidine ring moiety of the **14a** ligand extends further toward Leu278 than the
15
16 corresponding adenine group of the substrate analog. Because of this difference, mutation to the
17
18 larger phenylalanine amino acid could sterically hinder **14a** binding while leaving substrate and
19
20 transition state binding unaffected. By contrast, the structural overlap of the inhibitor and substrate
21
22 near the 437 position appears quite extensive in the structural alignment shown in **Figure 4**. As
23
24 the resistance-conferring mutations at this position introduce more polarity, it may be that
25
26 electrostatic forces play a large role in affording the differential effect on substrate/transition state
27
28 versus inhibitor binding. Further catalytic and inhibition studies as well as additional X-ray crystal
29
30 structures would be needed to understand the precise consequences of the resistance-conferring
31
32 mutations. These future studies may also reveal why **14e** MIC potency is not as largely affected
33
34 by the resistance-conferring mutations as the other inhibitors.
35
36
37
38
39
40
41
42
43
44
45
46
47
48
49
50
51
52
53
54
55
56
57
58
59
60

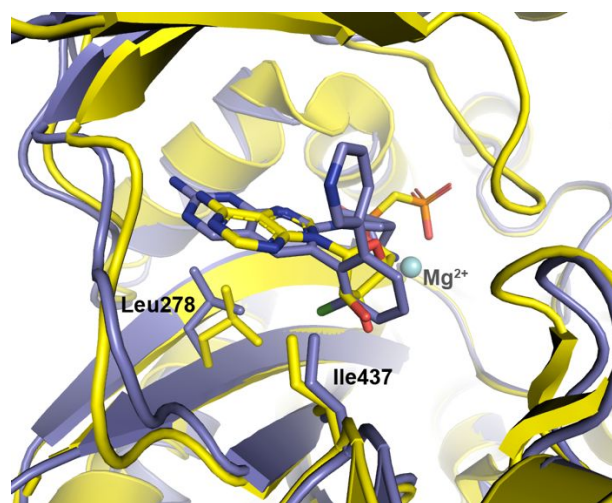


Figure 4. Alignment of the *P. aeruginosa* BC enzyme (shown in yellow ribbon; PBD 2VQD) co-crystallized with substrate analog AMPCP (carbon, yellow; nitrogen, blue; phosphate, orange; oxygen, red; all rendered as sticks) and the *H. influenzae* BC enzyme (shown in light blue ribbon) co-crystallized with **14a** (carbon, light blue; nitrogen, blue; chlorine, light green; all rendered as sticks; PDB code 6OI8). Resistance-conferring mutants were found at residue positions 278 and 437, which in the WT enzymes shown here are leucine and isoleucine, respectively (shown as sticks).

Additional resistant mutants were subjected to whole-genome sequencing to identify the underlying resistance mechanism. Several mutants were found to have mutations conferring single amino acid changes in MexT, which is a transcriptional regulator affecting many cellular processes.⁴⁸⁻⁵⁰ The effect of *mexT* mutation was highly compound-specific. Many BC inhibitors, including **14a** and **14e**, were unaffected by any *mexT* mutation (**Table 6**). However, the potency of **1** was reduced >8-fold by any of the three individual *mexT* mutations. The *mexT* mutants also had elevated resistance to ciprofloxacin and levofloxacin (data not shown), suggesting a general efflux-mediated mechanism is likely responsible for the observed phenotypes.

1
2
3 Sequencing also uncovered a large (647 kb) chromosomal inversion disrupting the coding
4 sequences of two efflux-related genes: *mexZ*, a repressor of *mexXY*, and *muxA*, which encodes the
5 periplasmic membrane fusion component of the MuxABC-OpmB efflux system. The disruption
6 presumably upregulates MexXY production while at the same time abrogates the function of
7 MuxABC-OpmB, but these hypotheses were not tested experimentally. The *muxA-mexZ* inversion
8 affected all tested BC inhibitors, reducing their potency 4- to 32-fold, and also reduced the potency
9 of ciprofloxacin and levofloxacin (data not shown), supporting the premise that resistance is
10 efflux-mediated. The lack of mutations in other pathways suggests that efflux and BC coding
11 mutations are the major resistance mechanisms for this set of compounds.
12
13
14
15
16
17
18
19
20
21
22
23
24
25

26 CONCLUSIONS

27
28 In this report, the physicochemical properties of starting compound **1** were rationally
29 optimized to improve Gram-negative cellular accumulation and BC target inhibition resulting in
30 the overall enhancement of antibacterial activity. Reducing the cLogD value and installing a
31 primary amine with a pK_a value in the physiological pH range resulted in compounds such as **14a**
32 and **14e**, which improved potency up to 64-fold against WT *E. coli*, 32-fold against WT *K.*
33 *pneumoniae*, and 16-fold against an efflux-compromised strain of *P. aeruginosa*.
34
35
36
37
38
39
40
41

42 While these MIC improvements demonstrate the potential of BC inhibitors as antibacterial
43 agents, several challenges remain. First, the understanding of the parameters affecting Gram-
44 negative penetration and efflux is still incomplete. For example, **13h** showed large MIC and cell
45 penetration improvements compared to the parent compound, despite having an almost identical
46 cLogD value. This observation lends further support to the conclusion drawn by more recent
47 studies that suggest cLogD is not as predictive of gram-Negative cellular accumulation as was
48
49
50
51
52
53
54
55
56
57
58
59
60

1
2
3 once proposed.²⁶ In addition, **14a**, one of the most potent compounds, still had rather large
4 decreases in MIC in the presence of PMBN and against efflux-compromised strains, indicating
5 that cell penetration and efflux are still significant barriers to the potency of this compound, despite
6 having “optimal” properties. These results suggest that there are other, as of yet, undiscovered
7 properties that likely contribute to penetration and efflux avoidance. Recent work has begun to
8 provide evidence that these other properties could likely include a molecule’s globularity and
9 number of rotatable bonds.^{26,29} In addition, the optimization strategy used here was largely
10 ineffective at improving potency against WT *A. baumannii* and *P. aeruginosa*. The unique
11 membrane composition and efflux mechanisms of these species may require different or additional
12 molecular properties to be satisfied before adequate antibacterial potencies can be achieved.
13
14
15
16
17
18
19
20
21
22
23
24
25

26 A second challenge illustrated by this work is the inherent resistance liability associated
27 with targets encoded by a single-copy gene like BC. All clinically relevant antibiotics overcome
28 this challenge by inhibiting targets encoded by multiple gene copies such as the ribosome
29 (aminoglycosides, macrolides, etc.) or multiple related targets such as penicillin binding proteins
30 (beta-lactams) and topoisomerases (quinolones) or by binding to non-protein targets (vancomycin,
31 polymyxins, etc.). The large MIC shifts observed herein from BC active-site mutations illustrate
32 the ease by which single amino acid changes can disrupt inhibitor binding without compromising
33 catalytic activity enough to jeopardize cell survival. In principle, if an inhibitor mimicked the
34 molecules along the catalytic pathway extensively enough, such single point mutations could not
35 arise. Designing such inhibitors has proved challenging but compounds such as **14e** with reduced
36 MIC shifts in the presence of BC active site mutations represent a promising starting point for
37 further optimization.
38
39
40
41
42
43
44
45
46
47
48
49
50
51
52
53
54
55
56
57
58
59
60

EXPERIMENTAL SECTION

Chemistry. All chemicals were purchased from commercial suppliers and used as received. Flash chromatography was carried out with prepacked silica cartridges from either ISCO or SiliCycle on an ISCO Companion chromatography system using gradient elution. NMR spectra were recorded on an Oxford 400 MHz spectrometer and referenced to tetramethylsilane. Preparative HPLC was performed on a Luna C18 5 μm column (50 mm 21 mm), eluting with mixtures of water acetonitrile. All final compounds were purified to >95% chemical purity, as assayed by HPLC with UV detection at $\lambda = 254$ and 210 nm.

Analytical LCMS was conducted on an Agilent 1200 series UPLC coupled with an Agilent G1946D Mass spectrometer and an Agilent 1200 DAD UV detector. All methods utilized the following parameters: Capillary voltage: 2500V; Fragmentor/Gain: 100; Gain: 1.0; Drying gas flow: 12.5 L/min; Gas Temperature: 350 $^{\circ}\text{C}$; Nebulizer Pressure: 60 psi; Scan Range: 100-1000 amu; Eluent A: 0.1% TFA in water; Eluent B: 0.1% TFA in acetonitrile; Flow: 0.8 mL/min; Column: Agilent SB-C18 RRHD 1.8 μm ; 2.1 x 50 mm; Column temperature: 35 $^{\circ}\text{C}$; LC retention times are based on the following methods: HPLC Method 1: Gradient: 2-50% eluent B over 2.0 minutes; HPLC Method 2: Gradient: 2-99% eluent B over 2.0 minutes; HPLC Method 3: Gradient: 2-30% eluent B over 2.0 minutes

2-[2-(3-pyridyl)phenyl]acetonitrile (2c): General procedure A: 2-(2-bromophenyl)acetonitrile (100 mg, 0.51 mmol), 3-pyridylboronic acid (130 mg, 1.0 mmol), potassium fluoride (60 mg, 1.0 mmol) were combined in 1,4-dioxane (3 mL) and methanol (0.90 mL) under nitrogen. $\text{Pd}_2(\text{dba})_3$ (9.3 mg, 0.010 mmol) and dicyclohexyl-[2-(2,6-dimethoxyphenyl)phenyl]phosphane (SPhos) (4.2 mg, 0.010 mmol) were added and the reaction was heated at 95 $^{\circ}\text{C}$ overnight. After cooling to

1
2
3 room temperature, the reaction was filtered and the filtrate was concentrated and used in the next
4
5 step without further purification (97 mg, 98%). LCMS (ESI) $[M+H]^+ = 195.0$.

6
7
8 **2-[2-chloro-6-(3-pyridyl)phenyl]acetonitrile (2d)** was prepared from 2-(2-bromo-6-chloro-
9
10 phenyl)acetonitrile (410 mg, 1.8 mmol) using general procedure A. The crude material was
11
12 purified by chromatography on silica gel, to yield the desired product (330 mg, 82%). LCMS (ESI)
13
14 $[M+H]^+ = 229.0$

15
16
17 **2-[2-chloro-6-(6-methoxy-3-pyridyl)phenyl]acetonitrile (2e)** was prepared using general
18
19 procedure A. The crude material was purified by RP-HPLC to yield the desired product (86 mg,
20
21 51%). LCMS (ESI) $[M+H]^+ = 259.0$

22
23
24 **2-(2-chloro-6-isobutoxy-phenyl)acetonitrile (2f)**. 2-chloro-6-hydroxy-benzaldehyde (1.0 g, 6.4
25
26 mmol) and isobutyl iodide (1.9 mL, 16 mmol) were combined in 8.0 ml anhydrous DMF, treated
27
28 with potassium carbonate (1.3 g, 9.6 mmol) and heated at 90 °C in a sealed vessel for two days.
29
30 The reaction was cooled to room temperature, diluted with water and extracted with ethyl acetate.
31
32 The ethyl acetate extract was washed with aqueous sodium metabisulfite solution and then brine
33
34 and concentrated under vacuum. The crude residue was purified on a silica gel column to give 2-
35
36 chloro-6-isobutoxybenzaldehyde (930 mg, 69%). LCMS (ESI) $[M+H]^+ = 213.0$.

37
38
39 A 200 ml round bottom flask fitted with addition funnel and nitrogen purged was charged with
40
41 potassium *tert*-butoxide (20% in THF, 10 mL, 18 mmol) and cooled in a -45 °C bath. A solution
42
43 of 1-Isocyanomethanesulfonyl-4-methyl-benzene (1.7 g, 8.8 mmol) in 12 ml anhydrous THF was
44
45 added dropwise over 10 min. After an additional 10 min, a solution of 2-chloro-6-isobutoxy-
46
47 benzaldehyde (930 mg, 4.4 mmol) in 12 ml THF was added dropwise over 10 min. After two hours
48
49 the reaction was allowed to warm to room temperature and then the solvent was removed under
50
51 vacuum. The residue was taken up in 30 ml water and acidified to pH 6 with 10% acetic acid. The
52
53
54
55
56
57
58
59
60

1
2
3 product was extracted with ethyl acetate (3 x 30 ml) and the combined extracts were washed with
4 saturated aqueous sodium bicarbonate and then brine, then dried over sodium sulfate, filtered and
5 concentrated under vacuum. The crude residue was purified on a silica gel column to give the
6 desired product (950 mg, 97%). LCMS (ESI) $[M+H]^+ = 223.9$.

7
8
9
10
11
12 **6-([1,1'-biphenyl]-2-yl)pyrido[2,3-d]pyrimidine-2,7-diamine (4b):** A solution of 2-([1,1'-
13 biphenyl]-2-yl)acetonitrile (34 mg, 0.17 mmol) in ethoxyethanol (0.5 mL) was treated with 25%
14 sodium methoxide in methanol (31 μ L, 0.14 mmol) followed by 2,4-diaminopyrimidine-5-
15 carbaldehyde (20 mg, 0.14 mmol) and then heated at 125 °C for 30 min. The reaction was diluted
16 with water and acidified with TFA. The solution was purified by RP-HPLC to give the desired
17 product (30 mg, 49%). HRMS (ESI) calculated $[M+H]^+ 314.1405$, found 314.1399; $^1\text{H NMR}$
18 (DMSO- d_6 , 400 MHz): δ 8.78 (1H, s), 7.84 (1H, s), 7.57 (1H, t, $J = 7.2$ Hz), 7.52 (1H, t, $J = 7.6$
19 Hz), 7.46 (1H, d, $J = 7.2$ Hz), 7.39 (1H, d, $J = 7.2$ Hz), 7.28–7.21 (5H, m).

20
21
22
23
24
25
26
27
28
29
30
31 **6-[2-(3-pyridyl)phenyl]pyrido[2,3-d]pyrimidine-2,7-diamine (4c):** General procedure B: A
32 solution of 2-[2-(3-pyridyl)phenyl]acetonitrile (97 mg, 0.50 mmol) in ethylene glycol (1.0 mL)
33 was treated with sodium methoxide (25% in methanol) (0.11 mL, 0.50 mmol) and 2,4-diamino-
34 pyrimidine-5-carbaldehyde (62 mg, 0.45 mmol). The reaction was heated at 140 °C for 2 h, then
35 cooled to rt, acidified with TFA (0.08 mL, 1 mmol) and purified by RP-HPLC to give the desired
36 product (65 mg, 30%). HRMS (ESI) calcd $[M+H]^+ 315.1358$, found 315.1355; $^1\text{H NMR}$ (DMSO-
37 d_6 , 400 MHz): δ 8.94 (1H, s), 8.04 (2H, d, $J = 8.0$ Hz), 7.93 (1H, s), 7.85 (3H, br s), 7.63–7.54
38 (4H, m), 7.48 (1H, t, $J = 6.8$ Hz), 1.96 (2H, br s), 1.75 (2H, br s).

39
40
41
42
43
44
45
46
47
48
49 **6-[2-chloro-6-(3-pyridyl)phenyl]pyrido[2,3-d]pyrimidine-2,7-diamine (4d).** was prepared
50 from 2-[2-chloro-6-(3-pyridyl)phenyl]acetonitrile (33 mg, 0.14 mmol) using general procedure B.
51 The crude material was purified by RP-HPLC to yield the desired product (10 mg, 15%). HRMS
52
53
54
55
56
57
58
59
60

(ESI) calcd $[M+H]^+$ 349.0968, found 349.0959; ^1H NMR (DMSO- d_6 , 400 MHz): δ 8.78 (1H, s), 8.43-8.41 (2H, m), 7.85 (1H, s), 7.72 (1H, dd, $J = 8.0, 0.4$ Hz), 7.65–7.60 (2H, m), 7.49 (1H, dd, $J = 8.0, 0.4$ Hz), 7.31 (1H, dd, $J = 7.6, 5.2$ Hz).

6-[2-chloro-6-(6-methoxy-3-pyridyl)phenyl]pyrido[2,3-d]pyrimidine-2,7-diamine (4e). was prepared using general procedure B (34 mg, 27%). HRMS (ESI) calcd $[M+H]^+$ 379.1074, found 379.1059; ^1H NMR (DMSO- d_6 , 400 MHz): δ 8.80 (1H, s), 8.02 (1H, d, $J = 2.4$ Hz), 7.86 (1H, s), 7.67 (1H, d, $J = 8.0$ Hz), 7.59 (1H, t, $J = 8.0$ Hz) 7.48 (1H, dd, $J = 8.8, 2.4$ Hz), 7.44 (1H, d, $J = 7.6$ Hz), 6.70 (1H, d, $J = 8.4$ Hz), 3.77 (3H, s).

6-(2-chloro-6-isobutoxy-phenyl)pyrido[2,3-d]pyrimidine-2,7-diamine (4f): A solution of 6-(2-chloro-6-isobutoxy-phenyl)-2-methylsulfinyl-pyrido[2,3-d]pyrimidin-7-amine (44 mg, 0.11 mmol) in 1.5 mL anhydrous THF was treated with 5M ammonia in methanol (0.45 mL, 2.3 mmol) and heated to 70 °C in a sealed vial overnight. The reaction was concentrated under vacuum and the crude residue was purified by RP-HPLC to give the desired product (23 mg, 60%). HRMS (ESI) calcd $[M+H]^+$ 344.1278, found 344.1276; ^1H NMR (DMSO- d_6 , 400 MHz): δ 8.90 (1H, s), 7.93 (1H, s), 7.46 (1H, t $J = 8.0$ Hz), 7.21 (1h, d, $J = 8.0$ Hz), 7.14 (1H, d, $J = 8.4$ Hz), 3.80–3.72 (2H, m), 1.86–1.81 (1H, m), 0.79 (6H, d, $J = 6.8$ Hz).

6-(2,6-dichlorophenyl)-2-methylsulfonyl-pyrido[2,3-d]pyrimidin-7-amine (6a): 4-amino-2-methylsulfonyl-pyrimidine-5-carbaldehyde (3.1 g, 18 mmol) was dissolved in 40 mL anhydrous dimethylformamide and cooled in an ice/methanol bath (–10 °C) for 15 minutes under nitrogen atmosphere. Sodium hydride (60% in mineral oil, 0.73 g, 18 mmol) divided into 5 portions was added over the course of 5 minutes keeping the reaction mixture cooled with stirring. After an additional 5 minutes a solution of 2,6-dichlorobenzylacetonitrile (4.9 g, 27 mmol) in 12 mL anhydrous dimethylformamide was added dropwise *via* syringe. The reaction mixture was stirred

1
2
3 at $-10\text{ }^{\circ}\text{C}$ for 30 minutes then allowed to warm to room temperature overnight after which time
4
5 the reaction mixture was cooled in an ice bath and slowly quenched with 50 mL saturated aqueous
6
7 ammonium chloride. After stirring for 20 minutes the product was extracted into DCM. The
8
9 combined DCM extracts were dried over anhydrous magnesium sulfate, filtered and concentrated
10
11 under reduced pressure. The residue was re-dissolved in ethyl acetate and washed with brine. The
12
13 organic layer was filtered through a sintered glass funnel and the filtrate was dried over anhydrous
14
15 sodium sulfate, filtered and concentrated under reduced pressure to dryness. The residue was
16
17 purified by silica gel chromatography eluting with ethyl acetate/dichloromethane to afford 710 mg
18
19 (11%) 6-(2,6-dichlorophenyl)-2-methylsulfanyl-pyrido[2,3-d]pyrimidin-7-amine LCMS (ESI):
20
21 $[\text{M}+\text{H}]^+ = 336.9$.

22
23
24
25
26 **6-[2-chloro-6-(3-pyridyl)phenyl]-2-methylsulfanyl-pyrido[2,3-d]pyrimidin-7-amine (6d):** 2-
27
28 [2-chloro-6-(3-pyridyl)phenyl]acetonitrile (210 mg, 0.94 mmol) was dissolved in DMF (3 mL)
29
30 and THF (1.5 mL) and cooled in an ice bath. Sodium hydride (60% in mineral oil, 39 mg, 0.98
31
32 mmol) was added followed by 4-amino-2-methylsulfanyl-pyrimidine-5-carbaldehyde (160 mg,
33
34 0.94 mmol) and the reaction was allowed to warm to rt. After stirring overnight, the reaction was
35
36 poured into ice and acidified to pH 4 with 10% aq. acetic acid. The product was extracted with
37
38 ethyl acetate (2 x) and the combined organics were washed with water and then brine and dried
39
40 with sodium sulfate, filtered and concentrated under reduced pressure. The oil was taken up in
41
42 DCM and purified by silica gel chromatography eluting with methanol/dichloromethane to afford
43
44 110 mg (30%) 6-[2-chloro-6-(3-pyridyl)phenyl]-2-methylsulfanyl-pyrido[2,3-d]pyrimidin-7-
45
46 amine LCMS (ESI): $[\text{M}+\text{H}]^+ = 380.0$.

47
48
49
50
51 **6-(2-chloro-6-isobutoxy-phenyl)-2-methylsulfanyl-pyrido[2,3-d]pyrimidin-7-amine (6f).** A
52
53 solution of 2-(2-chloro-6-isobutoxy-phenyl)acetonitrile (950 mg, 4.3 mmol) in 6 ml anhydrous
54
55
56
57
58
59
60

1
2
3 THF was cooled to $-10\text{ }^{\circ}\text{C}$ and treated with sodium hydride (60% in mineral oil, 200 mg, 4.9
4 mmol) (60% oil dispersion). After 10 min a solution of 4-amino-2-methylsulfanyl-pyrimidine-5-
5 carbaldehyde (720 mg, 4.3 mmol) in 14 mL anhydrous DMF was added dropwise over 10 min.
6
7
8 After 2h the reaction was warmed to $60\text{ }^{\circ}\text{C}$ and stirred overnight. After cooling to room
9
10
11 temperature, the reaction was diluted with water (30 mL) and extracted with ethyl acetate (3 x 75
12
13 mL). The combined extracts were washed with brine (3 x 30 mL), dried with sodium sulfate and
14
15 concentrated under vacuum. The crude residue was purified on a silica gel column to give the
16
17 desired product (950 mg, 60%). LCMS (ESI) $[\text{M}+\text{H}]^{+} = 375.0$.
18
19
20

21 **6-(2-chloro-6-isobutoxy-phenyl)-2-methylsulfinyl-pyrido[2,3-d]pyrimidin-7-amine (6g):** A
22
23 solution of 6-(2-chloro-6-isobutoxy-phenyl)-2-methylsulfanyl-pyrido[2,3-d]pyrimidin-7-amine
24
25 (43 mg, 0.11 mmol) in DCM (2 mL) was treated with 2-(benzenesulfonyl)-3-phenyl-oxaziridine
26
27 (30 mg, 0.11 mmol) and stirred overnight at rt. The reaction was concentrated under vacuum and
28
29 used directly in the next step. LCMS (ESI) $[\text{M}+\text{H}]^{+} = 391.0$.
30
31
32

33 **6-(2,6-dichlorophenyl)-2-methylsulfanyl-8H-pyrido[2,3-d]pyrimidin-7-one (7a):** 6-(2,6-
34
35 dichlorophenyl)-2-methylsulfanyl-pyrido[2,3-d]pyrimidin-7-amine (200 mg, 0.60 mmol) was
36
37 dissolved in TFA (5 mL) and cooled in an ice bath. Sodium nitrite (110 mg, 1.6 mmol) was added
38
39 and the reaction was stirred in the bath for 15 minutes, then at room temperature for 2.5 h, after
40
41 which time the reaction was slowly added to a mixture of saturated aqueous sodium bicarbonate,
42
43 solid sodium carbonate and ice (15-20 mL). The product was extracted with ethyl acetate (2 x 15
44
45 mL) and the combined organic layers were dried with sodium sulfate, filtered and concentrated
46
47 under vacuum giving 190 mg (96%) of 6-(2,6-dichlorophenyl)-2-methylsulfanyl-8H-pyrido[2,3-
48
49 d]pyrimidin-7-one LCMS (ESI): $[\text{M}+\text{H}]^{+} = 338.0$.
50
51
52
53
54
55
56
57
58
59
60

6-[2-chloro-6-(3-pyridyl)phenyl]-2-methylsulfanyl-8H-pyrido[2,3-d]pyrimidin-7-one (7d):

6-[2-chloro-6-(3-pyridyl)phenyl]-2-methylsulfanyl-pyrido[2,3-d]pyrimidin-7-amine (110 mg, 0.28 mmol) was dissolved in TFA (2 mL) and cooled in an ice bath. Sodium nitrite (52 mg, 0.75 mmol) was added and the reaction was allowed to warm to rt. After 90 min, the reaction was slowly added to a mixture of saturated aqueous sodium bicarbonate, solid sodium carbonate and ice. The product was extracted with ethyl acetate (2x) and the combined organics were washed with brine, dried with sodium sulfate, filtered and concentrated under reduced pressure to give 93 mg (88%) 6-[2-chloro-6-(3-pyridyl)phenyl]-2-methylsulfanyl-8H-pyrido[2,3-d]pyrimidin-7-one LCMS (ESI): $[M+H]^+ = 381.0$.

7-chloro-6-(2,6-dichlorophenyl)-2-methylsulfanyl-pyrido[2,3-d]pyrimidine (8a):

6-(2,6-dichlorophenyl)-2-methylsulfanyl-8H-pyrido[2,3-d]pyrimidin-7-one (190 mg, 0.57 mmol) was combined with phosphorous oxychloride (1.1 mL, 11 mmol) and dimethylformamide (1.0 μ L) at room temperature. The reaction was heated at 95 $^{\circ}$ C. An additional charge of phosphorous oxychloride (1.1 mL, 11 mmol) was added after 5 min. After 2 h, the phosphorous oxychloride was removed by concentration under reduced pressure. The residue was treated with ice and cold water in an ice bath to obtain a solid that was collected by filtration, rinsing with water. After further drying under vacuum, 200 mg (96%) of 7-chloro-6-(2,6-dichlorophenyl)-2-methylsulfanyl-pyrido[2,3-d]pyrimidine was obtained LCMS (ESI): $[M+H]^+ = 356.0$.

7-chloro-6-[2-chloro-6-(3-pyridyl)phenyl]-2-methylsulfanyl-pyrido[2,3-d]pyrimidine (8d):

6-[2-chloro-6-(3-pyridyl)phenyl]-2-methylsulfanyl-8H-pyrido[2,3-d]pyrimidin-7-one (93 mg, 0.24 mmol) phosphorous oxychloride (0.89 mL, 9.8 mmol) and dimethyl formamide (1.9 μ L, 0.020 mmol) were combined and stirred heated at 95 $^{\circ}$ C. After 4h, the reaction was concentrated under reduced pressure and dried further under high vacuum. The material was taken up in DCM

1
2
3 dripped slowly into ice cold sat. sodium bicarbonate. The layers were separated, and the aqueous
4 layer was extracted again with DCM. The combined organic layers were dried with sodium sulfate,
5
6 filtered and concentrated under reduced pressure to give 68 mg (70%) 7-chloro-6-[2-chloro-6-(3-
7
8 pyridyl)phenyl]-2-methylsulfanyl-pyrido[2,3-d]pyrimidine LCMS (ESI): $[M+H]^+ = 399.0$.

9
10
11 ***tert*-butyl *N*-[3-[6-(2,6-dichlorophenyl)-2-methylsulfanyl-pyrido[2,3-d]pyrimidin-7-yl]-3-**
12
13 **azabicyclo[3.1.0]hexan-6-yl]carbamate (10h):** 7-chloro-6-(2,6-dichlorophenyl)-2-
14
15 methylsulfanyl-pyrido[2,3-d]pyrimidine (35 mg, 0.10 mmol) was combined with acetonitrile (0.30
16
17 mL) 1,4-dioxane (0.30 mL), *tert*-butyl *N*-(3-azabicyclo[3.1.0]hexan-6-yl)carbamate (21 mg, 0.11
18
19 mmol) and *N,N'*-diisopropylethylamine (0.03 mL, 0.20 mmol) and the reaction was heated at 80
20
21 °C. Additional portions of diisopropylethylamine and *tert*-butyl *N*-(3-azabicyclo[3.1.0]hexan-6-
22
23 yl)carbamate were added and the temperature was increased to 90 °C. After heating overnight, the
24
25 solvent was removed by concentration under reduced pressure. The residue was taken up in DCM
26
27 (1 mL) and washed with 1M citric acid (2 x 1 mL), water, and sat. aqueous sodium bicarbonate,
28
29 then it was dried over sodium sulfate, filtered and concentrated under reduced pressure yielding
30
31 66 mg of crude *tert*-butyl *N*-[3-[6-(2,6-dichlorophenyl)-2-methylsulfanyl-pyrido[2,3-d]pyrimidin-
32
33 7-yl]-3-azabicyclo[3.1.0]hexan-6-yl]carbamate, which was taken forward without further
34
35 purification LCMS (ESI): $[M+H]^+ = 518.1$.

36
37
38 ***tert*-butyl *N*-[3-[6-(2,6-dichlorophenyl)-2-methylsulfinyl-pyrido[2,3-d]pyrimidin-7-yl]-3-**
39
40 **azabicyclo[3.1.0]hexan-6-yl]carbamate (11h):** *tert*-butyl *N*-[3-[6-(2,6-dichlorophenyl)-2-
41
42 methylsulfanyl-pyrido[2,3-d]pyrimidin-7-yl]-3-azabicyclo[3.1.0]hexan-6-yl]carbamate (51 mg,
43
44 0.10 mmol) was dissolved in DCM (1 mL) and 3-chloroperbenzoic acid (15 mg, 0.090 mmol) was
45
46 added at rt. After 2 h, the reaction was washed with sat. aqueous sodium bicarbonate, dried with
47
48 sodium sulfate, filtered and concentrated under reduced pressure to yield 60 mg of crude *tert*-butyl
49
50
51
52
53
54
55
56
57
58
59
60

1
2
3 *N*-[3-[6-(2,6-dichlorophenyl)-2-methylsulfinyl-pyrido[2,3-*d*]pyrimidin-7-yl]-3-
4 azabicyclo[3.1.0]hexan-6-yl]carbamate which was taken forward without further purification
5
6
7
8 LCMS (ESI): $[M+H]^+ = 534.0$.

9
10 **1-[2-amino-6-(2,6-dichlorophenyl)pyrido[2,3-*d*]pyrimidin-7-yl]pyrrolidine-3-carboxamide**
11
12 (**12a**) was prepared by the method in Scheme 2 using pyrrolidine-3-carboxamide hydrochloride in
13
14 step d and gaseous ammonia instead of 5 M ammonia in methanol in step f. HRMS (ESI) calculated
15
16 $[M+H]^+ 403.0841$, found 403.0822; $^1\text{H NMR}$ (DMSO-*d*₆, 400 MHz): δ 8.94 (1H, s), 7.91 (1H, s),
17
18 7.65-7.61 (2H, m), 7.51 (1H, t, *J* = 8.0 Hz), 7.41 (1H, s), 6.91 (1H, s), 2.90 (1H, br s), 2.02 (1H ,
19
20 br s), 1.91 (1H br s).

21
22
23 **[1-[2-amino-6-(2,6-dichlorophenyl)pyrido[2,3-*d*]pyrimidin-7-yl]pyrrolidin-3-yl]methanol**
24
25 (**12b**) was prepared by the method in Scheme 2 using pyrrolidin-3-ylmethanol in step d, gaseous
26
27 ammonia instead of 5 M ammonia in methanol in step f. HRMS (ESI) calculated $[M+H]^+ 390.0888$,
28
29 found 390.0883; $^1\text{H NMR}$ (DMSO-*d*₆, 400 MHz): δ 8.88 (1H, s), 7.85 (1H, s), 7.58 (1H, d, *J* =
30
31 4.0 Hz), 7.57 (1H, d, *J* = 3.6 Hz), 7.46 (1H, t, *J* = 8.0 Hz), 3.31–3.27 (2H, m), 3.21–3.18 (2H, m),
32
33 2.21 (1H, q, *J* = 6.8 Hz), 1.82–1.79 (1H, m), 1.60-1.55 (1H, m).

34
35
36
37 ***tert*-butyl *N*-[3-[2-amino-6-(2,6-dichlorophenyl)pyrido[2,3-*d*]pyrimidin-7-yl]-3-**
38
39 **azabicyclo[3.1.0]hexan-6-yl]carbamate (**12h**):** *tert*-butyl *N*-[3-[6-(2,6-dichlorophenyl)-2-
40
41 methylsulfinyl-pyrido[2,3-*d*]pyrimidin-7-yl]-3-azabicyclo[3.1.0]hexan-6-yl]carbamate (52 mg,
42
43 0.10 mmol) was dissolved in THF (2 mL) and ammonia (5 M in methanol) (0.49 mL, 2.5 mmol)
44
45 at rt. The reaction was then heated at 65 °C for 15 h, after which time the reaction was concentrated
46
47 to an oil to give crude *tert*-butyl *N*-[3-[2-amino-6-(2,6-dichlorophenyl)pyrido[2,3-*d*]pyrimidin-7-
48
49 yl]-3-azabicyclo[3.1.0]hexan-6-yl]carbamate which was used in the next step without further
50
51 purification LCMS (ESI): $[M+H]^+ = 487.0$.

1
2
3 **[3-amino-1-[2-amino-6-(2,6-dichlorophenyl)pyrido[2,3-d]pyrimidin-7-yl]pyrrolidin-3-**
4 **yl]methanol (13c)** was prepared by the method in Scheme 2 using *tert*-butyl *N*-[3-
5 (hydroxymethyl)pyrrolidin-3-yl]carbamate in step d and gaseous ammonia instead of 5 M
6 ammonia in methanol in step f. HRMS (ESI) calculated $[M+H]^+$ 405.0997, found 405.0979; ^1H
7 NMR (DMSO- d_6 , 400 MHz): δ 8.86 (1H, s), 8.14 (3H, br s), 7.83 (1H, s), 7.59 (2H, appt, $J = 8.4$
8 Hz), 7.47 (1H, t, $J = 8.0$ Hz), 5.63 (1H, s), 3.40–3.18 (8H, m), 2.07–2.00 (1H, m), 1.93–1.88 (1H,
9 m).

10
11
12
13
14
15
16
17
18
19 **7-[3-(aminomethyl)-3-fluoro-pyrrolidin-1-yl]-6-(2,6-dichlorophenyl)pyrido[2,3-**
20 **d]pyrimidin-2-amine (13d)** was prepared by the method in Scheme 2 using *tert*-butyl *N*-[(3-
21 fluoropyrrolidin-3-yl)methyl]carbamate in step d and gaseous ammonia instead of 5 M ammonia
22 in methanol in step f. HRMS (ESI) calculated $[M+H]^+$ 407.0954, found 407.0943; ^1H NMR
23 (DMSO- d_6 , 400 MHz): δ 8.85 (1H, s), 8.13 (3H, br s), 7.83 (1H, s), 7.61 (1H, d, $J = 8.0$ Hz), 7.57
24 (1H, d, $J = 8.0$ Hz), 7.47 (1H, t, $J = 8.4$ Hz), 3.78–3.68 (2H, m), 3.62 (1H, br s), 3.31 (2H, br s),
25 3.16 (1H, br s), 3.05 (1H, br s), 2.16–2.10 (1H, m), 2.06–2.01 (1H, m).

26
27
28
29
30
31
32
33
34
35 **1-[2-amino-6-(2,6-dichlorophenyl)pyrido[2,3-d]pyrimidin-7-yl]-3-(aminomethyl)pyrrolidin-**
36 **3-ol (13e)** was prepared by the method in Scheme 2 using *tert*-butyl *N*-[(3-hydroxypyrrrolidin-3-
37 yl)methyl]carbamate in step d and gaseous ammonia instead of 5 M ammonia in methanol in step
38 f. HRMS (ESI) calculated $[M+H]^+$ 405.0997, found 405.0982; ^1H NMR (DMSO- d_6 , 400 MHz): δ
39 8.87 (1H, s), 7.83 (3H, s), 7.64 (1H, d, $J = 8.0$ Hz), 7.61 (1H, d, $J = 8.4$ Hz), 7.51 (1H, t, $J = 8.0$
40 Hz), 2.92 (2H, s), 1.86 (2H, t, $J = 6.8$ Hz).

41
42
43
44
45
46
47
48
49 **7-[3-(aminomethyl)pyrrolidin-1-yl]-6-(2,6-dichlorophenyl)pyrido[2,3-d]pyrimidin-2-amine**
50 **(13f)** was prepared by the method in Scheme 2 using 3-(*N*-Boc-aminomethyl)pyrrolidine in step f
51 and gaseous ammonia instead of 5 M ammonia in methanol in step f. HRMS (ESI) calculated
52
53
54
55
56
57
58
59
60

1
2
3 [M+H]⁺ 389.1048, found 389.1035; ¹H NMR (DMSO-*d*₆, 400 MHz): δ 8.88 (1H, s), 7.85 (1H, s),
4
5 7.81 (3H, br s), 7.60-7.57 (2H, m), 7.47 (1H, t, *J* = 8.0 Hz), 3.57 (1H, br s), 3.07 (2H, br s), 2.82-
6
7 2.78 (1H, m), 2.75-2.70 (1H, m), 2.38-2.31 (1H, m), 1.96-1.92 (1H, m), 1.65-1.60 (1H, m).

9
10 **7-[4-(aminomethyl)-1-piperidyl]-6-(2,6-dichlorophenyl)pyrido[2,3-d]pyrimidin-2-amine**

11
12 **(13g)** was prepared by the method in Scheme 2 using *tert*-butyl *N*-(4-piperidinylmethyl)carbamate
13
14 in step d and 2-(benzenesulfonyl)-3-phenyl-oxaziridine instead of 3-chloroperbenzoic acid in step
15
16 e. HRMS (ESI) calculated [M+H]⁺ 403.1205, found 403.1188; ¹H NMR (DMSO-*d*₆, 400 MHz): δ
17
18 8.96 (1H, s), 7.94 (1H, s), 7.72-7.64 (5H, m), 3.92 (2H, br d, *J* = 12 Hz), 2.91 (2H, t, *J* = 12.8 Hz),
19
20 2.68 (2H, t, *J* = 6.4 Hz), 1.79 (1H, br s), 1.65 (2H, d, *J* = 11.6 Hz), 1.06 (2H, q, *J* = 10.0 Hz).
21
22

23
24 **7-((1*R*,5*S*,6*s*)-6-amino-3-azabicyclo[3.1.0]hexan-3-yl)-6-(2,6-dichlorophenyl)pyrido[2,3-**

25
26 **d]pyrimidin-2-amine (13h):** *tert*-butyl *N*-[3-[2-amino-6-(2,6-dichlorophenyl)pyrido[2,3-
27
28 d]pyrimidin-7-yl]-3-azabicyclo[3.1.0]hexan-6-yl]carbamate (48 mg, 0.10 mmol) was dissolved in
29
30 DCM (0.50 mL) and TFA (0.50 mL) at room temperature. After 45 minutes, the reaction was
31
32 concentrated under vacuum. The residue was taken up in dimethylformamide and purified by
33
34 reverse phase HPLC (1'' Phenomenex Luna column, 0.1% TFA in water/ACN) to afford 18 mg
35
36 (35% over four steps) 7-[(1*R*,5*S*)-6-amino-3-azabicyclo[3.1.0]hexan-3-yl)-6-(2,6-
37
38 dichlorophenyl)pyrido[2,3-d]pyrimidin-2-amine. HRMS (ESI) calculated [M+H]⁺ 387.0891,
39
40 found 387.0886; ¹H NMR (DMSO-*d*₆, 400 MHz): δ 8.83 (1H, s), 8.04 (3H, br s), 7.77 (1H, s), 7.59
41
42 (2H, d, *J* = 8.0 Hz), 7.48 (1H, t, *J* = 8.4 Hz), 3.42-3.33 (4H, m), 2.15 (1H, s), 1.95 (2H, s).
43
44
45
46
47
48
49
50
51
52
53
54
55
56
57
58
59
60

7-[(1R,5S)-6-amino-3-azabicyclo[3.1.0]hexan-3-yl)-6-[2-chloro-6-(3-

pyridyl)phenyl]pyrido[2,3-d]pyrimidin-2-amine (14a). The compound was prepared according to the procedure for **12a**, to give 17 mg of **14a** HRMS (ESI) calcd $[M+H]^+$ 430.1547, found 430.1525; ^1H NMR (DMSO- d_6 , 400 MHz): δ 8.88 (1H, s), 8.41 (1H, d, $J = 6.4$ Hz), 8.31 (1H, d, $J = 2$ Hz), 8.05 (3H s), 7.89 (1H, s), 7.74 (1H, d, $J = 7.6$ Hz), 7.63 (1H, t, $J = 8.0$ Hz), 7.49 (1H, d, $J = 7.6$ Hz), 7.44 (1H, d, $J = 8.0$ Hz), 7.25 (1H, dd, $J = 7.6, 4.8$ Hz), 3.34 (1H, br s), 3.21–3.16 (2H, m), 2.09 (1H, br s), 1.95 (2H, br s).

7-[(1R,5S)-6-amino-3-azabicyclo[3.1.0]hexan-3-yl)-6-[2-chloro-6-(4-

pyridyl)phenyl]pyrido[2,3-d]pyrimidin-2-amine (14b) The compound was prepared according to the procedure for **14c**: HRMS (ESI) calculated $[M+H]^+$ 430.1547, found 430.1526; ^1H NMR (DMSO- d_6 , 400 MHz): δ 8.88 (1H, s), 8.44 (2H, d, $J = 5.6$ Hz), 8.06 (3H, br s), 7.87 (1H, s), 7.76 (1H, d, $J = 7.2$ Hz), 7.65 (1H, t, $J = 7.6$ Hz), 7.50 (1H, d, $J = 7.2$ Hz), 7.09 (2H, d, $J = 4.8$ Hz), 2.12 (1H, s), 1.96 (2H, s).

7-[(1R,5S)-6-amino-3-azabicyclo[3.1.0]hexan-3-yl)-6-[2-chloro-6-(5-fluoro-6-methoxy-3-

pyridyl)phenyl]pyrido[2,3-d]pyrimidin-2-amine (14c): *tert*-butyl *N*-[3-[2-amino-6-(2-bromo-6-chloro-phenyl)pyrido[2,3-d]pyrimidin-7-yl]-3-azabicyclo[3.1.0]hexan-6-yl]carbamate (15 mg, 0.030 mmol) 1,4-dioxane (0.60 mL), 1 M sodium carbonate (0.15 mL), (5-fluoro-6-methoxy-3-pyridyl)boronic acid (5.3 mg, 0.030 mmol) and Pd(dppf)Cl₂ DCM complex (2.3 mg, 0.0028 mmol) were combined in a vial under nitrogen at rt. The reaction was stirred at 100 °C for 1h. The product was extracted with ethyl acetate and the combined organic layers were dried with sodium sulfate, filtered and concentrated under reduced pressure to give 20 mg of crude *tert*-butyl *N*-[3-[2-amino-6-[2-chloro-6-(5-fluoro-6-methoxy-3-pyridyl)phenyl]pyrido[2,3-d]pyrimidin-7-yl]-3-

azabicyclo[3.1.0]hexan-6-yl]carbamate that was used in the next step without further purification.

LCMS (ESI): $[M+H]^+ = 578.1$.

The compound was prepared according to the procedure for **13h**. HRMS (ESI) calculated $[M+H]^+$ 478.1558, found 478.1538; ^1H NMR (DMSO- d_6 , 400 MHz): δ 8.84 (1H, s), 8.06 (3H, br s), 7.84 (1H, s), 7.71 (2H, appd, $J = 7.2$ Hz), 7.60 (1H, t, $J = 7.6$ Hz), 7.47 (1H, d, $J = 7.6$ Hz), 7.39 (1H, d, $J = 11.2$ Hz), 3.86 (3H, s), 2.08 (1H, s), 1.94 (2H, s).

7-[(1R,5S)-6-amino-3-azabicyclo[3.1.0]hexan-3-yl)-6-[2-chloro-6-(2-methylthiazol-5-yl)phenyl]pyrido[2,3-d]pyrimidin-2-amine (14d) The compound was prepared according to the procedure for **14c** HRMS (ESI) calculated $[M+H]^+$ 450.1267, found 450.1254; ^1H NMR (DMSO- d_6 , 400 MHz): δ 8.84 (1H, s), 8.02 (3H, br s), 7.76–7.73 (3H, m), 7.65 (1H, d, $J = 8.0$ Hz), 7.57 (1H, t, $J = 8.0$ Hz) 2.03 (1H, s), 1.95 (2H, s).

7-[(1R,5S)-6-amino-3-azabicyclo[3.1.0]hexan-3-yl)-6-(2-chloro-6-isobutoxy-phenyl)pyrido[2,3-d]pyrimidin-2-amine (14e). The compound was prepared according to the procedure for **12a**: HRMS (ESI) calculated $[M+H]^+$ 425.1856, found 425.1843, ^1H NMR (DMSO- d_6 , 400 MHz): δ 8.89 (1H, s), 8.07 (3H, s), 7.75 (1H, s), 7.43 (1H, t, $J = 8.4$ Hz), 7.18 (1H, d, $J = 8.0$ Hz), 7.08 (1H, d, $J = 8.4$ Hz), 3.77–3.69 (3H, m), 3.35 (4H, br s), 2.11 (1H, s), 1.98 (2H, s), 1.79–1.76 (1H, m), 0.76–0.70 (6H, m).

Bacterial Strains. Wild type strains of *A. baumannii* (ATCC 19606) and *K. pneumoniae* (ATCC 43816) were obtained from the American Type Culture Collection. The *E. coli* ΔtolC knockout was constructed at Achaogen in the DM4100 background (Coli Genetic Stock Center Database #6333). The *P. aeruginosa* efflux-compromised strain $\Delta\text{mexAB-oprM}::\text{Cm } \Delta\text{mexEF-oprN}::\Omega\text{Hg } \Delta\text{mexCD-oprJ}::\text{Gm}$, also known as PAM1262, was constructed in a PAO1 background as described in Ref. **47** and kindly provided by the authors.

1
2
3
4
5 **Minimum Inhibitory Concentrations.** MICs were determined by broth microdilution according
6
7 to guidelines established by the Clinical and Laboratory Standards Institute.⁵¹ Compounds were
8
9 serially diluted in two-fold increments in 100% DMSO, then diluted 10-fold in water. Inocula were
10
11 prepared from cells streaked onto Mueller Hinton agar (MHA) and grown at 35 °C overnight. 10
12
13 μL of antibiotic solution was mixed with 90 μL of inoculum in cation-adjusted Mueller Hinton
14
15 broth in 96-well assay plates, with a final inoculum of approximately 5×10^4 cells/well. When
16
17 included, PMBN was diluted in broth prior to addition of cells, to a final assay concentration of 8
18
19 $\mu\text{g}/\text{mL}$. After incubation of assay plates at 35 °C for 18-20 hours, the lowest concentration of
20
21 antibiotic that prevented visible growth was recorded as the MIC. In general, MIC values reported
22
23 are geometric means of at least two independent measurements rounded to the nearest standard
24
25 dilution increment.
26
27
28
29
30
31
32

33 **Purification of *P. aeruginosa* BC.** The acetyl-CoA carboxylase (*accC*) gene was cloned from *P.*
34
35 *aeruginosa* (PAO1) genomic DNA using forward primer with underlined EcoR1 restriction site
36
37 5'- GACTGAATTCTATGTTGGAAAAAGTGCTGATCG-3' and reverse primer with SacI
38
39 restriction site 5'-GACTGAGCTCTCAGTGCTTGTCCATACCC-3' and inserted into the
40
41 pET47b(+) expression vector (Novagen). This construct has the following N-terminal sequence
42
43 preceding the WT BC sequence: MAHHHHHHSAALEVLFGPGYQDPNS. Recombinant N-
44
45 terminal His-Tagged BC was overexpressed in Rosetta™(DE3)pLysS *E. coli* cells (Novagen). A
46
47 starter culture of 25 mL of LB broth containing kanamycin (50 $\mu\text{g}/\text{mL}$) and chloramphenicol (34
48
49 $\mu\text{g}/\text{mL}$) was inoculated with a single colony of the Rosetta™(DE3)pLysS *E. coli* cells containing
50
51 the His-Tagged BC construct and grown overnight at 37 °C. 20 mL of starter culture was used to
52
53
54
55
56
57
58
59
60

1
2
3 inoculate 2 L of LB broth containing kanamycin (50 $\mu\text{g}/\text{mL}$) and chloramphenicol (34 $\mu\text{g}/\text{mL}$).
4
5 The culture was grown to an OD_{600} of 0.5 at 37 $^{\circ}\text{C}$ at which point 0.5 nM IPTG was added to
6
7 induce overexpression for 3 hours. Cells were then pelleted at 10,200 g for 15 minutes and
8
9 resuspended in 10 mL of Buffer A (20 mM Tris \cdot HCl, pH 7.9, 500 mM NaCl, and 5 mM imidazole).
10
11 The resulting cell slurry was lysed either by sonication (duty cycle 30; power 6, pulse for 15 sec,
12
13 rest for 45 seconds for 20 rounds on ice) or using an Avestin Emulsiflex. The lysed solution was
14
15 then centrifuged at 75,000 g for at least 1 hour. The supernatant was gravity flowed over a 3mL
16
17 Co^{2+} His-binding column (Pierce) and incubated with the resin for 30 minutes with rotation at 4
18
19 $^{\circ}\text{C}$. The column was washed with 30 mL of Buffer A and then 10 mL of Buffer B (20 mM
20
21 Tris \cdot HCl, pH 7.9, 500 mM NaCl, and 170 mM imidazole) was added to the column to elute the
22
23 protein. The eluent was exchanged into Buffer C (10 mM HEPES, pH 8.0, 25 mM KCl, and 1 mM
24
25 TCEP) using 10,000 MWCO filters (Amicon $^{\circledR}$) or dialysis. The buffer exchanged sample (5 mL)
26
27 was applied to a 5 mL Q-Sepharose column (GE Healthcare) at 2 mL/min. After a 50 mL wash
28
29 with Buffer C, protein was eluted with a linear gradient over 50 mL of Buffer D (10 mM HEPES,
30
31 pH 8.0, 250 mM KCl, and 1 mM TCEP). Fractions were collected and assessed using SDS-PAGE
32
33 (12 % gel; Bio-Rad). Fractions containing the desired BC at >95% purity were pooled and
34
35 exchanged into 10 mM HEPES, pH 7.0, 500 mM KCl using an Amicon $^{\circledR}$ 10,000 MWCO filtration
36
37 unit. A bicinchoninic acid assay (Pierce $^{\text{TM}}$) was used to determine the final protein concentration.
38
39
40
41
42
43
44

45 Previously reported purification procedures were used to purify material for the X-ray
46
47 crystallography studies^{18,37}
48
49
50
51

52 ***P. aeruginosa* BC enzyme assay.** The IC_{50} assay used to measure a compound's relative inhibition
53
54 of *P. aeruginosa* BC was adapted from the coupled assay reported by Ref. 5. The previous study
55
56
57
58
59
60

1
2
3 used the full ACCase multi-enzyme complex consisting of BC, carboxytransferase, and biotin
4 carboxyl carrier protein, while the assay herein uses only the isolated BC enzyme. Both BC and
5 ACCase catalytic activities produce inorganic phosphate (**Figure S1**), which in the IC₅₀ assay is
6 coupled to the generation of a spectroscopically active product. However, because the k_{cat} and K_{M}
7 values for inorganic phosphate generation by ACCase likely differs from BC in isolation, the
8 apparent IC₅₀ values measured for a given inhibitor of the two different enzyme preparations are
9 not directly comparable.
10
11
12
13
14
15
16
17
18

19 Initial rates of BC activity were measured at various concentrations of test inhibitor in 96-
20 well plates with a final reaction volume of 300 μL . An initial solution was made such that the final
21 concentration of each component would be 50 mM HEPES, pH 8.0, 100 mM KCl, 1 mM TCEP,
22 5 mM MgCl₂, 0.1 mg/mL BSA, 0.005% (vol/vol) Tween 20, 150 μM 7-methyl-6-thioguanosine
23 (Barry and Associates), 0.25 U/mL purine nucleoside phosphorylase (Sigma), 2 mM ATP, 10 mM
24 sodium carbonate, and 50 mM biotin. This solution was incubated at room temperature for 30
25 minutes. Afterwards, purified *P. aeruginosa* BC was added to achieve a final apparent
26 concentration of 15 nM and 270 μL of the resulting solution was distributed into the wells of a 96-
27 well plate containing 30 μL of a 10X concentration of test inhibitor (previously diluted in <1%
28 DMSO) in 3-fold serial dilutions across the plate row. Reaction progress was monitored by the
29 increase in absorbance at 360 nm. Initial rates at each inhibitor compound were plotted and fitted
30 to a standard IC₅₀ equation.
31
32
33
34
35
36
37
38
39
40
41
42
43
44
45
46
47
48
49

50 **Crystallization and Data Collection.** Crystallization conditions are summarized in **Table S1**.
51
52 Diffraction data were collected at 100 K at the 24-ID-E beamline equipped with a CCD-based
53 ADSC Quantum 315 detector. The images were processed using the XDS program suit⁵² and
54
55
56
57
58
59
60

1
2
3 scaled using the Scala program.⁵³ Data collection and data processing statistics are given in **Table**
4
5 **S1**.

6
7
8
9
10 **Crystal Structure Determination.** The molecular replacement procedure was applied to locate a
11 solution for the **13f** data set using the program Phaser.⁵⁴ A monomer of *E. coli* BC (PDB ID: 2V58)
12 was used as a search model. The positioned MR model was refined using the maximum likelihood
13 refinement in REFMAC⁵⁵ with the TLS parameters generated by the TLSMD server.⁵⁶ Program
14 Coot⁵⁷ was used for model building throughout the refinement. The final model consists of protein
15 residues 1-447 (molecule A), 1-447 (molecule B), two **13f** molecules, 3 ethylene glycol molecules,
16 and 432 water molecules. Alternate conformations have been built for protein residues S68, E71,
17 N90, R111, K116, S118, R314, R423 (mol A) and I5, R37, R314 (mol B).
18
19
20
21
22
23
24
25
26
27

28 A monomer of *H. influenzae* BC (PDB: 4RZQ) was used as a search model to locate a
29 solution for the **14a** data set. The positioned MR solution was refined as described above. The final
30 model consists of protein residues 1-445, one **14a** molecule, one ethylene glycol molecule, and 30
31 water molecules.
32
33
34
35
36
37
38
39

40 **Bacterial Cytological Profiling.** Cultures of *E. coli* (ATCC 25922) were grown in LB at 30 °C to
41 an OD₆₀₀ ~0.15. Cultures were then split and each sample treated with the test compound for 120
42 minutes. The cells were stained with FM 4-64 (membranes), DAPI (DNA), and Sytox Green (cell
43 integrity). Cells were then imaged at 100X magnification using an Applied Precision DeltaVision
44 Deconvolution microscope.
45
46
47
48
49
50
51
52
53
54
55
56
57
58
59
60

1
2
3 **Resistance Frequency.** Spontaneous resistance frequency was measured by plating approximately
4
5 10^9 colony-forming units from 5 independent cultures of the efflux-compromised strain of *P.*
6
7 *aeruginosa* onto MHA containing **1** at 4-, 8-, and 16-fold above the MIC. The inoculum density
8
9 of each culture was determined by plating serial dilutions onto drug-free MHA. Plates were
10
11 incubated at 35 °C in ambient air. After 48 hours, visible colonies on antibiotic-containing plates
12
13 were counted, and several colonies from each plate were archived for MIC analysis and
14
15 sequencing. The frequency for each culture and antibiotic level was calculated as the number of
16
17 colonies on the antibiotic-containing plate divided by the inoculum density for that culture. The
18
19 reported frequency is the mean of the frequencies from the five independent cultures.
20
21
22
23
24
25

26 **Genome Sequencing.** Whole-genome sequences of the *P. aeruginosa* efflux-compromised parent
27
28 and the wild type ancestral strain were determined on a PacBio RSII system at the Arizona
29
30 Genomics Institute and assembled into single contigs. Both genomes were re-sequenced by
31
32 Illumina HiSeq (read length 2 x 100 base pairs) to resolve minor homopolymer discrepancies,
33
34 resulting in a high-quality reference genome for the parent strain. Spontaneous mutants were
35
36 sequenced by Illumina HiSeq. Raw reads were filtered for quality, trimmed, and assembled against
37
38 the reference genome by Maverix Biomics. Single-nucleotide variants were reported by Maverix
39
40 Biomics and verified at Achaogen by inspection of the assembled reads for representative mutants
41
42 of each class. The inversion junction sites in *muxA* and *mexZ* were determined by analysis of the
43
44 assembled reads.
45
46
47
48
49
50

51 **ASSOCIATED CONTENT**

52
53
54
55
56
57
58
59
60

1
2
3 **Supporting Information:** Figure S1 showing the reaction catalyzed by BC and the acyl-CoA
4 carboxylase multienzyme complex; Text S1 describing the tests of BC essentiality in *P.*
5 *aeruginosa*; Table S1 of X-ray crystallographic conditions and statistics; molecular formula strings
6
7
8
9

10
11
12 **PDB ID Codes:** The coordinates for X-ray co-crystal structures of **13f** and **14a** have been
13 deposited in the PDB with codes 6OI9 and 6OI8, respectively.
14
15
16
17

18 19 **AUTHOR INFORMATION**

20 21 **Corresponding Author(s):**

22
23 *L.D.A.; E-mail, logdrewn@gmail.com
24
25

26 *R.T.C.; E-mail, ryancirz@gmail.com
27

28 29 **ORCID**

30 Logan D. Andrews: 0000-0002-5092-4530
31

32 Ryan T. Cirz: 0000-0002-9848-7421
33
34
35
36

37 **Author Contributions:** All authors have given approval to this manuscript
38
39
40
41

42 **Notes:** The authors declare no competing financial interest.
43
44
45

46 47 **ACKNOWLEDGEMENTS**

48
49 Research reported in this publication was supported by the National Institute of Allergy and
50 Infectious Diseases of the National Institutes of Health under Award Number R21AI113572. We
51 acknowledge Andrew McCandlish for help preparing and managing grant applications. This report
52 also includes research conducted at the Northeastern Collaborative Access Team beam lines
53
54
55
56
57
58
59
60

1
2
3 (24ID-C and 24ID-E at the Advanced Photon Source), which are funded by the National Institute
4 of General Medical Sciences (P41 GM103403) from the National Institutes of Health. The Pilatus
5 6M detector on 24ID-C is funded by an NIH-ORIP HEI grant (S10 RR029205) and use of the
6 Advanced Photon Source, an Office of Science User Facility operated for the U.S. Department of
7 Energy by Argonne National Laboratory, is under Contract No. DE-AC02-06CH11357. The
8 content is solely the responsibility of the authors and does not necessarily represent the official
9 views of the National Institutes of Health. We acknowledge the computational modeling and
10 scientific advice of Erin Bradley and the microbiological assay contributions of Hoan Lee.
11
12
13
14
15
16
17
18
19
20
21
22

23 **ABBREVIATIONS**

24
25
26 ICU, intensive care unit; INV, inversion; MIC, minimum inhibitory concentration; K, Kelvin; BC,
27 biotin carboxylase; IC, inhibitory concentration; ATCC, American Type Culture Collection; CLSI,
28 Clinical and Laboratory Standards Institute; MHA, Mueller-Hinton agar; PMBN, polymyxin B
29 nonapeptide; DMSO, dimethyl sulfoxide; ATP, adenosine triphosphate; HTS, high-throughput
30 screen; MR, molecular replacement; US, United States; LB, lysogeny broth; AMPCP, adenosine
31 5'-(alpha,beta-methylene)diphosphate; IPTG, Isopropyl β -D-1-thiogalactopyranoside; TCEP,
32 tris(2-carboxyethyl)phosphine; MWCO, molecular weight cut off; lipopolysaccharide, LPS
33
34
35
36
37
38
39
40
41
42
43
44
45
46
47
48
49
50
51
52
53
54
55
56
57
58
59
60

REFERENCES

(1) *Antibiotic Resistance Threats in the United States, 2013*. U.S. Centers for Disease Control and Prevention. [Online] <http://www.cdc.gov/drugresistance/threat-report-2013>. (accessed Feb 27, 2019).

(2) Burnham, J.; Olsen, M.; Kollef, M. Re-Estimating Annual Deaths Due to Multidrug-Resistant Organism Infections. *Infection Control and Hospital Epidemiology*. **2019**, *40*, 112-113.

(3) Cassini, A.; Hogberg, L. D.; Plachouras, D.; Quattrocchi, A.; Hoxha, A.; Simonsen, G. S.; Colomb-Cotinat, M.; Kretzschmar, M. E.; Devleeschauwer, B.; Cecchini, M.; Ouakrim, D. A.; Oliveira, T. C.; Struelens, M. J.; Suetens, C.; Monnet, D. L.; Burden of AMR Collaborative Group. Attributable Deaths and Disability-Adjusted Life-Years Caused by Infections with Antibiotic-Resistant Bacteria in the EU and the European Economic Area in 2015: a Population-Level Modelling Analysis. *Lancet Infect. Dis.* **2019**, *19*, 56-66

(4) Chen, L.; Todd, R.; Kiehlbauch, J.; Walters, M.; Kallen, A. Notes From the Field: Pan-Resistant New Delhi Metallo-Beta-Lactamase-Producing *Klebsiella pneumoniae* - Washoe County, Nevada, 2016. *MMWR Morb. Mortal Wkly. Rep.* **2017**, *66*, 33.

(5) Miller, J. R.; Dunham S.; Mochalkin, I.; Banotai, C.; Bowman, M.; Buist, S.; Dunkle, B.; Hanna, D.; Harwood, H. J.; Huband, M. D.; Karnovsky, A.; Kuhn, M.; Limberakis, C.; Liu, J. Y.; Mehrens, S.; Mueller, W. T.; Narasimhan, L.; Ogden, A.; Ohren, J.; Prasad, J. V. N. V.; Shelly, J. A.; Skerlos, L.; Sulavik, M.; Thomas, V. H.; VanderRoest, S.; Wang, L.; Wang, Z.; Whitton, A.; Zhu, T.; Stover, C. K. A Class of Selective Antibacterials Derived From a Protein Kinase Inhibitor Pharmacophore. *Proc. Natl. Acad. Sci. USA.* **2009**, *106*, 1737-1742.

1
2
3 (6) Payne, D. J.; Warren, P. V.; Holmes, D. J.; Ji, Y.; Lonsdale, J. T. 2001. "Bacterial Fatty-
4 Acid Biosynthesis: A Genomics-Driven Target for Antibacterial Drug Discovery." *Drug Discov.*
5 *Today*. **2001**, *6*, 537-544.
6
7

8
9
10 (7) Campbell, J. W.; Cronan, J. E. Jr. 2001. Bacterial Fatty Acid Biosynthesis: Targets for
11 Antibacterial Drug Discovery. *Annu. Rev. Microbiol.* **2001**, *55*, 305-332.
12
13

14 (8) Heath, R. J.; White, S. W.; Rock, C. O. Lipid Biosynthesis as a Target for Antibacterial
15 Agents. *Prog. Lipid Res.* **2001**, *40*, 467-497.
16
17

18 (9) Zhang, Y. M.; White, S. W.; Rock, C. O. Inhibiting Bacterial Fatty Acid Synthesis. *J.*
19 *Biol. Chem.* **2006**, *281*, 17541-17544.
20
21

22 (10) Wright, H. T.; Reynolds K. A. Antibacterial Targets in Fatty Acid Biosynthesis. *Curr.*
23 *Opin. Microbiol.* **2007**, *10*, 447-453.
24
25

26 (11) Parsons, J. B.; Rock, C. O. Is Bacterial Fatty Acid Synthesis a Valid Target for
27 Antibacterial Drug Discovery? *Curr. Opin. Microbiol.* **2011**, *14*, 544-549.
28
29

30 (12) Cronan, J. E. Jr.; Waldrop, G. L. Multi-Subunit Acetyl-CoA Carboxylases. *Prog. Lipid*
31 *Res.* **2002**, *41*, 407-435.
32
33

34 (13) Mochalkin, I.; Miller, J. R.; Narasimhan, L.; Thanabal, V.; Erdman, P.; Cox, P. B.;
35 Prasad, J. V.; Lightle, S.; Huband, M. D.; Stover, C. K. Discovery of Antibacterial Biotin
36 Carboxylase Inhibitors by Virtual Screening and Fragment-Based Approaches. *ACS Chem. Biol.*
37 **2009**, *4*, 473-483.
38
39

40 (14) Cheng, C. C.; G. W. Jr. Shipps; Z. Yang; B. Sun; N. Kawahata; K. A. Soucy; A.
41 Soriano; Orth, P.; Xiao, L.; Mann, P.; Black, T. Discovery and Optimization of Antibacterial
42 AccC Inhibitors. *Bioorg. Med. Chem. Lett.* **2009**, *19*, 6507-6514.
43
44
45
46
47
48
49
50
51
52
53
54
55
56
57
58
59
60

1
2
3 (15) Ogden, A.; Kuhn, M.; Dority, M.; Buist, S.; Mehrens, S.; Zhu, T.; Xiao, D.; Miller, J.
4 R.; Hanna, D. Evaluation of Pharmacokinetic/Pharmacodynamic Relationships of PD-0162819, a
5 Biotin Carboxylase Inhibitor Representing a New Class of Antibacterial Compounds, Using *In*
6 *Vitro* Infection Models. *Antimicrob. Agents Chemother.* **2012**, *56*, 124-129.
7
8

9
10
11 (16) Silvers, M. A.; Robertson, G. T.; Taylor, C. M.; Waldrop, G. L.. Design, Synthesis, and
12 Antibacterial Properties of Dual-Ligand Inhibitors of Acetyl-CoA Carboxylase. *J. Med. Chem.*
13 **2014**, *57*, 8947-8959.
14
15

16
17 (17) Wallace, J.; Bowlin, N. O.; Mills, D. M.; Saenkham, P.; Kwasny, S. M.; Opperman, T.
18 J.; Williams, J. D.; Rock, C. O.; Bowlin, T. L.; Moir, D. T. Discovery of Bacterial Fatty Acid
19 Synthase Type II Inhibitors Using a Novel Cellular Bioluminescent Reporter Assay. *Antimicrob.*
20 *Agents Chemother.* **2015**, *59*, 5775-5787.
21
22

23
24 (18) Mochalkin, I.; Miller, J. R.; Evdokimov, A.; Lightle, S.; Yan, C.; Stover, C. K.;
25 Waldrop, G. L. Structural Evidence for Substrate-Induced Synergism and Half-Sites Reactivity
26 in Biotin Carboxylase. *Protein Sci.* **2008**, *17*, 1706-1718.
27
28

29 (19) Nikaido, H.; Vaara, M. 1985. Molecular Basis of Bacterial Outer Membrane
30 Permeability. *Microbiol. Rev.* **1985**, *49*, 1-32.
31
32

33 (20) Nikaido, H. Prevention of Drug Access to Bacterial Targets: Permeability Barriers and
34 Active Efflux. *Science.* **1994**, *264*, 382-388.
35
36

37 (21) Kumar, A.; Schweizer, H. P. Bacterial Resistance to Antibiotic: Active Efflux and
38 Reduced Uptake. *Adv. Drug Deliv. Rev.* **2005**, *57*, 1486-1513.
39
40

41 (22) Brown, D. G.; May-Dracka, T. L.; Gagnon, M. M.; Tommasi, R. Trends and Exceptions
42 of Physical Properties on Antibacterial Activity for Gram-Positive and Gram-Negative
43 Pathogens. *J. Med. Chem.* **2014**, *57*, 10144-10161.
44
45
46
47
48
49
50
51
52
53
54
55
56
57
58
59
60

1
2
3 (23) Tommasi, R.; Brown, D. G.; Walkup, G. K.; Manchester, J. I.; Miller, A. A.
4
5 ESKAPEing the Labyrinth of Antibacterial Discovery. *Nat. Rev. Drug Discov.* **2015**, *14*, 529-
6
7 542.
8

9
10 (24) Mugumbate, G.; Overington, J. P. The Relationship Between Target-Class and the
11
12 Physicochemical Properties of Antibacterial Drugs. *Bioorg. Med. Chem.* **2015**, *23*, 5218-5224.
13

14 (25) O'Shea, R.; Moser, H. E. Physicochemical Properties of Antibacterial Compounds:
15
16 Implications for Drug Discovery. *J. Med. Chem.* **2008**, *51*, 2871-2878.
17
18

19 (26) Richter, M. F.; Drown, B. S.; Riley, A. P.; Garcia, A.; Shirai, T.; Svec, R. L.;
20
21 Hergenrother, P. J. Predictive Rules for Compound Accumulation Yield a Broad-Spectrum
22
23 Antibiotic. *Nature*, **2017**, *545*, 299-304.
24
25

26 (27) Serio, A. W.; Kubo, A.; Lopez, S.; Gomez, M.; Corey, V. C.; Andrews, L. D.; Schwatz,
27
28 M. A.; Kasar, R.; McEnRoe, G.; Aggen, J.; Miller, G.; Armstrong, E. S. Structure, Potency and
29
30 Bactericidal Activity of ACHN-975, a First-In-Class LpxC Inhibitor. *53rd Interscience*
31
32 *Conference on Antimicrobial Agents and Chemotherapy*, **2013** [poster #F-1226].
33
34

35 (28) Tari, L. W.; M. Trzoss; D. C. Bensen; X. Li; Z. Chen; T. Lam; J. Zhang; Creighton, C.
36
37 J.; Cunningham, M. L.; Kwan, B.; Stidham, M.; Shaw, K. J.; Lightstone, F. C.; Wong, S. E.;
38
39 Nguyen, T. B.; Nix, J.; Finn, J. Pyrrolopyrimidine Inhibitors of DNA Gyrase B (GyrB) and
40
41 Topoisomerase IV (ParE). Part I: Structure Guided Discovery and Optimization of Dual
42
43 Targeting Agents with Potent, Broad-Spectrum Enzymatic Activity. *Bioorganic and Medicinal*
44
45 *Chemistry Letters*, **2013**, *23*, 1529-1536.
46
47
48

49 (29) Richter, M. F.; Hergenrother, P. J. The Challenge of Converting Gram-Positive-Only
50
51 Compounds Into Broad-Spectrum Antibiotics. *Ann. N. Y. Acad. Sci.* **2019**, *1435*, 18-38.
52
53
54
55
56
57
58
59
60

1
2
3 (30) Vaara, M. Agents That Increase the Permeability of the Outer Membrane. *Microbiol.*
4 *Rev.* **1992**, *56*, 395-411.

7 (31) Angus, B. L.; Carey, A. M.; Caron, D. A.; Kropinski, A. M.; Hancock, R. E. Outer
8 Membrane Permeability in *Pseudomonas aeruginosa*: Comparison of a Wild-Type with an
9 Antibiotic-Supersusceptible Mutant. *Antimicrob. Agents Chemother.* **1982**, *21*, 299-309.

14 (32) Yoshimura, F.; Nikaido, H. Permeability of *Pseudomonas aeruginosa* Outer Membrane
15 to Hydrophilic Solutes. *J. Bacteriol.* **1982**, *152*, 636-642.

19 (33) Delcour, A. H. Outer Membrane Permeability and Antibiotic Resistance. *Biochim.*
20 *Biophys. Acta* **2009**, *1794*, 808-816.

24 (34) Page, M. G. The Role of the Outer Membrane of Gram-Negative Bacteria in Antibiotic
25 Resistance: Ajax's Shield or Achilles' Heel? *Handb. Exp. Pharmacol.* **2012**, *211*, 67-86.

28 (35) Breidenstein, E. B.; de la Fuente-Nunez, C.; Hancock, R. E. *Pseudomonas aeruginosa*:
29 All Roads Lead to Resistance. *Trends Microbiol.* **2011**, *19*, 419-426.

33 (36) Waldrop, G. L.; Holden, H. M.; St. Maurice, M. The Enzymes of Biotin Dependent CO₂
34 Metabolism: What Structures Reveal About Their Reaction Mechanisms. *Protein Sci.* **2012**, *21*,
35 1597-1619.

39 (37) Broussard, T. C.; Pakhomova, S.; Neau, D. B.; Bonnot, R.; Waldrop, G. L. Structural
40 Analysis of Substrate, Reaction Intermediate, and Product Binding in *Haemophilus influenzae*
41 Biotin Carboxylase. *Biochemistry*, **2015**, *54*, 3860-3870.

46 (38) Cunningham, M. L.; Kwan, B. P.; Nelson, K. J.; Bensen, D. C.; Shaw, K. J..
47 Distinguishing On-Target Versus Off-Target Activity in Early Antibacterial Drug Discovery
48 Using a Macromolecular Synthesis Assay. *Journal of Biomolecular Screening*, **2013**, *18*, 1018-
49 1026.

1
2
3 (39) Nonejuie, P.; Burkart, M.; Pogliano, K.; Pogliano, J. Bacterial Cytological Profiling
4 Rapidly Identifies the Cellular Pathways Targeted by Antibacterial Molecules. *Proc. Natl. Acad.*
5 *Sci. U.S.A.* **2013**, *110*, 16169-16174.
6
7

8
9
10 (40) Lamsa, A.; Liu, W. T.; Dorrestein, P. C.; Pogliano, K. The *Bacillus subtilis* Cannibalism
11 Toxin SDP Collapses the Proton Motive Force and Induces Autolysis. *Mol. Microbiol.* **2012**, *84*,
12 486-500.
13
14

15
16
17 (41) Lamsa, A.; Lopez-Garrido, J.; Quach, D.; Riley, E. P.; Pogliano, J.; Pogliano, K.. 2016.
18 Rapid Inhibition Profiling in *Bacillus subtilis* to Identify the Mechanism of Action of New
19 Antimicrobials. *ACS Chem. Biol.* **2016**, *11*, 2222-2231.
20
21

22
23
24 (42) Mohammad, H.; W. Younis; L. Chen; C. E. Peters; J. Pogliano; K. Pogliano; B. Cooper;
25 Zhang, J.; Mayhoub, A.; Oldfield, E.; Cushman, M.; Seleem, M. N. Phenylthiazole Antibacterial
26 Agents Targeting Cell Wall Synthesis Exhibit Potent Activity *In Vitro* and *In Vivo* Against
27 Vancomycin-Resistant Enterococci. *J. Med. Chem.* **2017**, *60*, 2425-2438.
28
29

30
31
32 (43) Lin, L.; Nonejuie, P.; Munguia, J.; Hollands, A.; Olson, J.; Dam, Q.; Kumaraswamy,
33 M.; Rivera, H. Jr.; Corriden, R.; Rohde, M.; Hensler, M. E.; Burkart, M. D.; Pogliano, J.;
34 Sakoulas, G.; Nizet, V. Azithromycin Synergizes with Cationic Antimicrobial Peptides to Exert
35 Bactericidal and Therapeutic Activity Against Highly Multidrug-Resistant Gram-Negative
36 Bacterial Pathogens. *EBioMedicine*, **2015**, *2*, 690-698.
37
38

39
40
41 (44) Nonejuie, P.; Trial, R. M.; Newton, G. L.; Lamsa, A.; Ranmali Perera, V.; Aguilar, J.;
42 Liu, W. T.; Dorrestein, P. C.; Pogliano, J.; Pogliano, K. Application of Bacterial Cytological
43 Profiling to Crude Natural Product Extracts Reveals the Antibacterial Arsenal of *Bacillus*
44 *subtilis*. *J. Antibiot. (Tokyo)*, **2016**, *69*, 353-361.
45
46
47
48
49
50
51
52
53
54
55
56
57
58
59
60

1
2
3 (45) Hamby, J. M.; Connolly, J. C.; Schroeder, M. C.; Winters, R. T.; Showalter, H. D. H.;
4
5 Panek, R. L.; Major, T. C.; Olsewski, B.; Ryan, M. J.; Dahring, T.; Lu, G. H.; Keiser, J.; Amar,
6
7 A.; Shen, C.; Kraker, A. J.; Slintak, V.; Nelson, J. M.; Fry, D. W.; Bradford, L.; Hallak, H.;
8
9 Doherty, A. M. Structure-Activity Relationships for a Novel Series of Pyrido[2,3-d]pyrimidine
10
11 Tyrosine Kinase Inhibitors. *J. Med. Chem.* **1997**, *40*, 2296-2303.
12
13

14 (46) Hernandez, V.; Crepin, T.; Palencia, A.; Cusack, S.; Akama, T.; Baker, S. J.; Bu, W.;
15
16 Feng, L.; Freund, Y. R.; Liu, L.; Meewan, M.; Mohan, M.; Mao, W.; Rock, F. L.; Sexton, H.;
17
18 Sheoran, A.; Zhang, Y.; Zhang Y. K.; Zhou, Y.; Nieman, J. A.; Anugula, M. R.; Keramane, el
19
20 M.; Savariraj, K.; Reddy, D. S.; Sharma, R.; Subedi, R.; Singh, R.; O'Leary, A.; Simon, N. L.;
21
22 De Marsh, P. L.; Mushtaq, S.; Warner, M.; Livermore, D. M.; Alley, M. R.; Plattner, J. J.
23
24 Discovery of Novel Class of Boron-Based Antibacterials with Activity Against Gram-Negative
25
26 Bacteria. *Antimicrob. Agents Chemother.* **2013**, *57*, 1394-1403.
27
28
29

30 (47) Lomovskaya, O.; Lee, A.; Hoshino, K.; Ishida, H.; Mistry, A.; Warren, M. S.; Boyer, E.;
31
32 Chamberland, S.; Lee, V. J. Use of a Genetic Approach to Evaluate the Consequences of
33
34 Inhibition of Efflux Pumps in *Pseudomonas aeruginosa*. *Antimicrob. Agents Chemother.* **1999**,
35
36 *43*, 1349-1346.
37
38

39 (48) Tian, Z. X.; Mac Aogain, M.; O'Connor, H. F.; Fargier, E.; Mooji, M. J.; Adams, C.;
40
41 Wang, Y. P.; O'Gara, F. MexT Modulates Virulence Determinants in *Pseudomonas aeruginosa*
42
43 Independent of the MexEF-OprN Efflux Pump. *Microb. Pathog.* **2009**, *47*, 237-241.
44
45

46 (49) Tian, Z. X.; Fargier, E.; Mac Aogain, M.; Adams, C.; Wang, Y. P.; O'Gara, F.
47
48 Transcriptome Profiling Defines a Novel Regulon Modulated by the LysR-Type Transcriptional
49
50 Regulator MexT in *Pseudomonas aeruginosa*. *Nucleic Acids Res.* **2009**, *37*, 7546-7559.
51
52
53
54
55
56
57
58
59
60

1
2
3 (50) Luong, P. M.; Shogan, B. D.; Zaborin, A.; Belogortseva, N.; Shrout, J. D.; Zaborina, O.;
4 Alverdy, J. C. Emergence of the P2 Phenotype in *Pseudomonas aeruginosa* PAO1 Strains
5 Involves Various Mutations in MexT or MexF. *J. Bacteriol.* **2014**, *196*, 504-513.
6
7

8
9
10 (51) CSLI. *Methods for Dilution Antimicrobial Susceptibility Tests for Bacteria That Grow*
11 *Aerobically; Approved Standard-Tenth Edition*. CSLI document M07-A10. Wayne, PA: Clinical
12 and Laboratory Standards Institute; 2015.
13
14

15
16
17 (52) Kabsch, W. XDS. *Acta Crystallogr. D Biol. Crystallogr.* **2010**, *66(Pt 2)*, 125-132.
18

19 (53) Evans, P. Scaling and Assessment of Data Quality. *Acta Crystallogr. D Biol.*
20 *Crystallogr.* **2006**, *62(Pt 1)*, 72-82.
21
22

23 (54) Adams, P. D.; Afonine, P. V.; Bunkoczi, G.; Chen, V. B.; Davis, I. W.; Echols, N.;
24 Headd, J. J.; Hung, L. -W.; Kapral, G. J.; Grosse-Kunstleve, R. W.; McCoy, A. J.; Moriarty, N.
25 W.; Oeffner, R.; Read, R. J.; Richardson, D. C.; Richardson, J. S.; Terwilliger, T. C.; Zwart, P.
26 H. PHENIX: A Comprehensive Python-Based System for Macromolecular Structure Solution.
27 *Acta Crystallogr. D Biol. Crystallogr.* **2010**, *66(Pt 2)*, 213-221.
28
29
30
31
32

33 (55) Collaborative Computation Project, Number 4. The CCP4 Suite: Programs for Protein
34 Crystallography. *Acta Crystallogr. D Biol. Crystallogr.* **1994**, *50(Pt 5)*, 760-763.
35
36
37

38 (56) Painter, J.; Merritt, E. A. TLSMD Web Server for the Generation of Multi-Group TLS
39 Models. *J. Appl. Cryst.* **2006**, *39*, 109-11.
40
41
42

43 (57) Emsley, P.; Cowtan, K. Coot: Model-Building Tools for Molecular Graphics. *Acta*
44 *Crystallogr. D Biol. Crystallogr.* **2004**, *60(Pt 12 Pt 1)*, 2126-2132
45
46
47
48
49
50
51
52
53
54
55
56
57
58
59
60

TABLE OF CONTENTS GRAPHIC

